Cell Transplantation, Vol. 14, pp. 695–700, 2005

0963-6897/05 $20.00 + .00
E-ISSN 1555-3892
www.cognizantcommunication.com

Time Course Evaluation of Reparative Cartilage With MR Imaging After Autologous Chondrocyte Implantation

Atsuya Watanabe,*† Yuichi Wada,* Takayuki Obata,† Takahisa Sasho,* Takuya Ueda,‡ Mitsuru Tamura,† Hiroo Ikehira,† and Hideshige Moriya*

*Department of Orthopaedic Surgery, Graduate School of Medicine, Chiba University, Chiba, 260-8677 Japan
†National Institute of Radiological Sciences, Chiba, 263-8555 Japan
‡Department of Radiology, Graduate School of Medicine, Chiba University, Chiba, 260-8677 Japan

The aim of this study was to evaluate the qualitative change in reparative cartilage after autologous chondrocyte implantation (ACI). Ten knees of 10 patients were studied. The signal intensities of reparative and normal cartilage were evaluated by fat-suppressed three-dimensional spoiled-gradient recalled (FS 3D-SPGR) MR imaging. The signal intensity (SI) index (signal intensity of reparative cartilage divided by that of normal cartilage) was defined and the change in SI index was investigated. Histological and biochemical evaluation was done at the second look arthroscopy. The SI index was at its lowest level immediately after ACI and increased with time to 9 months thereafter. After 9–12 months, the SI index settled to almost level and was maintained at that value for at least 2–3 years postoperatively. The average of the SI indexes after 12 months to the last examination was 74.2 ± 4.6 (range 64.2–82.8), which means signal intensity of reparative cartilage was maintained at a value lower than that of normal cartilage. The total ICRS score was 11.6 ± 2.3 points (mean ± SD). The GAG concentration was 107.9 ± 17.0 μg/mg (mean ± SD) in normal cartilage and 65.9 ± 9.4 μg/mg in reparative cartilage. The quality of reparative cartilage as hyaline cartilage was inferior to that of normal cartilage. In the present study, the time course change in the SI index indicates that the major maturation process of implanted chondrocytes neared completion in 9–12 months. Minor changes, such as matrix remodeling with reorganization of the collagen fibers in reparative cartilage, may continue, but an almost identical condition seemed to be maintained during the first 2–3 years of follow-up. SI index does not always reflect all properties of reparative cartilage but may be a useful parameter for noninvasive evaluation.

Key words: Autologous chondrocyte implantation; Magnetic resonance imaging; Time course evaluation; Signal intensity; Reparative cartilage

INTRODUCTION

Autologous chondrocyte implantation (ACI) has recently become a widely used technique for articular cartilage lesions. Formerly, it was known as an effective, essential treatment, especially for the large osteochondral defects of knee articular cartilage (15).

Until now, most follow-up studies of ACI treatment in humans have been conducted by using clinical assessments; however, only a few follow-up studies concerning the qualitative aspect of reparative cartilage have been conducted (15). One of the reasons for the small number of follow-up studies has been that the qualitative evaluation of reparative cartilage could be achieved only by invasive methods, such as arthroscopy with biopsy.

The aim of this study was to evaluate the time course change of quality in reparative cartilage after ACI by using magnetic resonance (MR) imaging. We performed fat-suppressed three-dimensional spoiled-gradient recalled (FS 3D-SPGR) MR imaging to investigate the changes of signal intensity in reparative cartilage. With this imaging technique, normal articular cartilage appears higher in signal intensity than adjacent structures (6). Histological and biochemical evaluation of reparative cartilage was done at the second-look arthroscopy to assess how closely the reparative cartilage resembled normal cartilage.

MATERIALS AND METHODS

The knees of 10 patients (seven males and three females) were investigated after the patients had undergone ACI of the femoral condyle (seven medial femoral

Address correspondence to Atsuya Watanabe, Department of Orthopaedic Surgery, Graduate School of Medicine, Chiba University, 1-8-1, Inohana, Chuo-Ku, Chiba-Shi, 260-8677 Japan. Tel: 81-43-226-2117; Fax: 81-43-226-2116; E-mail: atsuyan1@pa2.so-net.ne.jp

condyles and three lateral femoral condyles). The patients' mean age at the time of ACI was 21.2 ± 7.5 years (range 13–35 years), and the mean size of the defect was 4.5 ± 2.1 cm^2 (range 2.3–10.5 cm^2). This study was approved by the ethics review committee of Chiba University Hospital, and informed consent was obtained from all patients.

ACI was performed according to the method described by Brittberg and colleagues (3). In brief, healthy cartilage was obtained from a non-weight-bearing area of the affected knee during an initial arthroscopy. Chondrocytes were then isolated from the cartilage and cultured in the laboratory for about 4 weeks (Genzyme Tissue Repair, Cambridge, MA). The cultured chondrocytes were injected into the defect, which was covered by a periosteal flap that had been removed from the tibia. The rehabilitation schedule included active movement of the knee, which was started immediately after surgery. Weight bearing was gradually introduced at 6 weeks after ACI and increased to full weight bearing by 10 weeks after ACI.

FS 3D-SPGR MR imaging was performed in the sagittal plane at 0, 3, 6, 9, 12, 18, 24, and 36 months after ACI using an MR imaging system at 1.5 Tesla with a dedicated knee coil (Signa Horizon General Electronic, Milwaukee, WI) (In three cases, imaging was performed up to 24 months.) The scanning parameters were 52 ms repetition time, 10 ms echo time, 60° flip angle, 130 × 130 mm field of view, 1.5 mm section thickness, and 512 × 512 matrix. To compare the signal intensity of reparative cartilage with that of normal cartilage over time, we defined the signal intensity (SI) index (signal intensity of reparative cartilage divided by the signal intensity of normal cartilage) and expressed it as a percentage. We investigated the change in SI index during the observation period.

It is known that the signal intensity on MR images by FS 3D-SPGR imaging is given by the equation:

$$SI = \{k \cdot \rho[1 - \exp(-TR/T_1)]\sin\alpha\}/[1 - \cos\alpha \cdot \exp(-TR/T_1)]$$

where k is the constant factor determined by the imaging apparatus, ρ is proton density, α is flip angle, TR is repetition time, and T_1 is longitudinal relaxation time.

The T_1 of articular cartilage may vary depending on the histological and biochemical characteristics of the cartilage. With this imaging technique, a strong T_1 weighted image is obtained and signal intensity is considered to mainly reflect the tissue-specific T_1 when the imaging apparatus and scanning parameters are the same. To verify that the signal intensity of reparative cartilage and normal cartilage in FS 3D-SPGR MR images represented the T_1 of the two cartilages, T_1 measurements were performed.

T_1 measurements were performed at 21.2 ± 10.4 months (range 13–38 months) after ACI by using a MR imaging system at 1.5 Tesla (Gyroscan Intera; Philips Medical Systems, Holland). A time course T_1 measurement was also performed for a patient at 1, 4, 8, 12, 18, and 24 months after ACI. Inversion recovery turbo-spin echo images were obtained at six inversion times: 50, 100, 200, 400, 800, and 1600 ms. The scanning parameters were 1800 ms repetition time, 28 ms echo time, 130 × 130 mm field of view, 3.0 mm section thickness, 512 × 512 matrix, and 6 turbo spin echo factor. T_1 calculated maps were generated from inversion recovery images, using the commercially available software, Dr. View (Asahikasei; Tokyo, Japan), and the T_1s of reparative cartilage and normal cartilage were investigated. We investigated the change of T_1 in the patient who underwent time course T_1 measurement.

For the signal intensity and T_1 measurements, the region of interest (ROI) was drawn in the whole area of reparative cartilage. The hypertrophic periosteum (if it existed) was not included in the ROI. The ROI of normal cartilage was drawn in the weight-bearing area of the femoral condyle about 2 cm apart from the reparative cartilage (to avoid including the damaged cartilage near reparative cartilage). To standardize the procedure, all ROIs were drawn by the same investigator.

A second-look arthroscopy with biopsy was performed at 12.3 ± 0.5 months (range 12–13 months) after ACI surgery. Using an 11-gauge biopsy needle (Trapsystem MDTECH, Gainesville, FL), we took biopsies from all cases of reparative cartilage and from seven cases of normal cartilage. Reparative cartilage was stained with hematoxylin and eosin (H&E) and toluidine blue (TB) for general histology and the assessment of metachromasia. The International Cartilage Repair Society (ICRS) assessment form for repair of cartilage (14) was used to score the histological appearance of reparative cartilage (Table 1). The concentration of glycosaminoglycan (GAG), a major macromolecular constituent of articular cartilage, that was obtained from biopsy was evaluated with high-performance liquid chromatography in nine cases of reparative cartilage and seven cases of normal cartilage.

The Lysholm score (13) was performed to quantify the clinical status of the patients before ACI, 1 year after ACI, and at the time of the last evaluation (30.6 ± 8.9 months, range 18–47 months, after the ACI).

A t-test was used for statistical evaluation and significant difference was defined as $p < 0.05$.

RESULTS

In the MR images of a typical case, the signal intensity of reparative cartilage appeared low immediately after ACI, but it increased and approached that of normal cartilage with time (Fig. 1).

In all cases, the SI index fell to its lowest level imme-

Table 1. ICRS Visual Histological Assessment Scale

Feature	Score
1. Surface	
Smooth/continuous	3
Discontinuities/irregularities	0
2. Matrix	
Hyaline	3
Mixture: hyaline/fibrocartilage	2
Fibrocartilage	1
Fibrous tissue	0
3. Cell distribution	
Columnar	3
Mixed/columnar-clusters	2
Clusters	1
Individual cells/disorganized	0
4. Cell population viability	
Predominantly viable	3
Partially viable	2
<10% viable	0
5. Subchondral bone	
Normal	3
Increased remodeling	2
Bone necrosis/granulation tissue	1
Detached/fracture/callus at base	0
6. Cartilage mineralization (calcified cartilage)	
Normal	3
Abnormal/inappropriate location	0

diately after ACI but increased rapidly for 9 months thereafter. After 9–12 months, the SI index settled to almost level and was maintained at that value for at least 2–3 years postoperatively (Fig. 2). The average of the SI indexes from 12 months to the last examination was 74.2 ± 4.6 (range 64.2–82.8). This average means that the signal intensity of reparative cartilage was maintained at a value lower than that of normal cartilage.

The T_1 of reparative cartilage was significantly higher than that of normal cartilage, 1.34 ± 0.13 and 1.03 ± 0.08 s, respectively ($p < 0.05$). The T_1 in the patient who underwent time course T_1 measurement was at its highest level immediately after ACI, decreased with time to 9 months, and settled to almost level after that, which was compatible with the change of SI index (Fig. 3).

The average ICRS score of each criteria (see Table 1) was: 1) 1.2 ± 1.5 points, 2) 2.5 ± 0.7 points, 3) 1.6 ± 0.5 points, 4) 1.4 ± 0.8 points, 5) 1.9 ± 0.3 points, 6) 3.0 ± 0 points; the total was 11.6 ± 2.3 points. The histological appearance of reparative cartilage after ACI was not as good as that of normal cartilage.

The GAG concentration obtained from biopsy was 107.9 ± 17.0 μg/mg in normal cartilage and 65.9 ± 9.4 μg/mg in reparative cartilage. This difference in concentration was statistically significant ($p < 0.05$). In fact, the GAG concentrations of reparative cartilage were lower than normal cartilage in all cases.

There was a significant improvement in patients' Lysholm scores from a mean of 63.0 ± 12.2 points before surgery to 94.9 ± 5.1 points 1 year after surgery, and 97.7 ± 4.9 points at the time of the last evaluation.

DISCUSSION

The T_1 in cartilage may be shortened by decreased water content, increased concentration of macromolecular matrix components, and increased regularity of the collagen network structure (9). The time course change in the SI index that we observed may have been caused by changes in T_1 during the maturing process of the transplanted chondrocytes from the state of suspension to hard hyaline-like cartilage. Indeed, the T_1 in reparative cartilage decreased with time after grafting in this

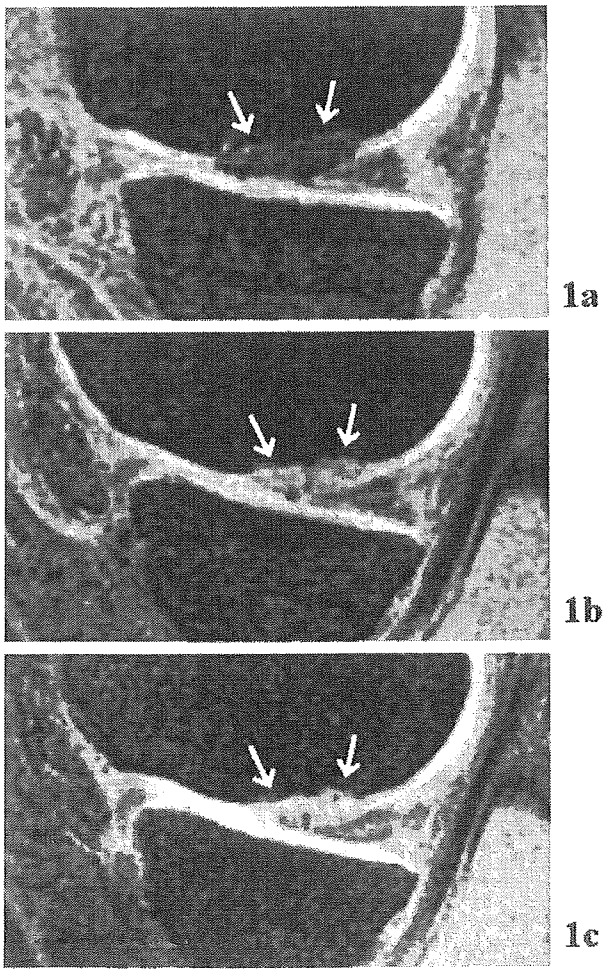

Figure 1. The time course change of signal intensity in three-dimensional spoiled gradient-recalled (3D-SPGR) magnetic resonance (MR) images of a typical case. The signal intensity of reparative cartilage (arrows) appeared low immediately after autologous chondrocytes implantation (ACI), but it increased and approached that of normal cartilage with time. (a) MR image immediately after ACI, (b) MR image 3 months after ACI, (c) MR image 12 months after ACI.

study. In simple words, as the reparative cartilage became more compatible with normal hyaline cartilage, the SI index increased. The SI index does not always reflect all properties of reparative cartilage but may be a useful parameter of changes in reparative cartilage in noninvasive evaluation.

Several animal studies on ACI concerning time course change of reparative cartilage have been done. However, differences in the outcomes between animals studied have been shown. For example, in a rabbit study, the reparative tissue appeared to mature towards hyaline cartilage for about 3 months, and an almost identical condition was maintained after that (4). In contrast, in a canine study, the reparative tissue appeared to mature for about 3–6 months, but the reparative cartilage appeared to become progressively damaged after that (1). Why there should be this apparent difference between animal species is unclear. In humans, the literature contains only a few reports that focus on the time course of cartilage maturation. The main maturation process of implanted cartilage in humans is believed to near completion within 1 year after implantation (10,11,17). In the present study, the time course change in the SI index that we observed indicates that the major maturation process of implanted chondrocytes neared completion in 9–12 months. We also observed that the quality of reparative cartilage as hyaline cartilage was inferior to that of normal cartilage. Minor changes, such as matrix remodeling with reorganization of the collagen fibers in reparative cartilage, may continue, but an almost identical condition was maintained during the first 2–3 years of follow-up. This is similar to the impression obtained from clinical results that it reached nearly full marks 1 year after operation and was maintained until the time of the final observation.

Evaluation of the maturation process of reparative cartilage is important in determining postoperative treatment such as adjustment of weight bearing and restrictions of activity. Evaluation of reparative cartilage after maturation is also important in assessing treatment results and predicting outcomes such as the presence or absence of long-term degenerative changes. This study suggested that the first 9 months after ACI were important because the histological success of reparative cartilage might be determined. Adjustments of the postoperative treatment, which could influence maturation of the reparative tissue, during this period could result in making reparative cartilage that is closer to normal hyaline cartilage.

Histology of reparative cartilage after ACI has been

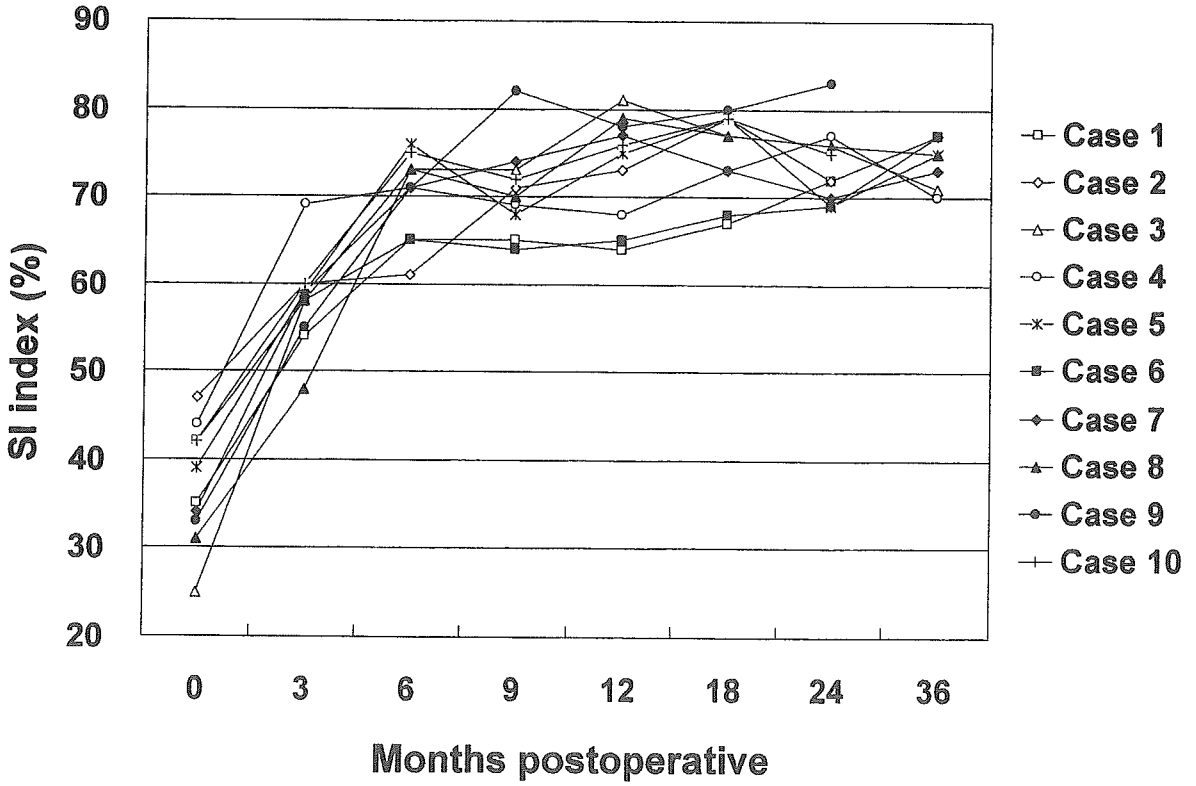

Figure 2. The signal intensity (SI) index after autologus chondrocytes implantation. The SI index was at its lowest level immediately after ACI and increased with time to 9 months thereafter. After 9–12 months, the SI index settled to almost level and was maintained at that value for at least 2–3 years postoperatively.

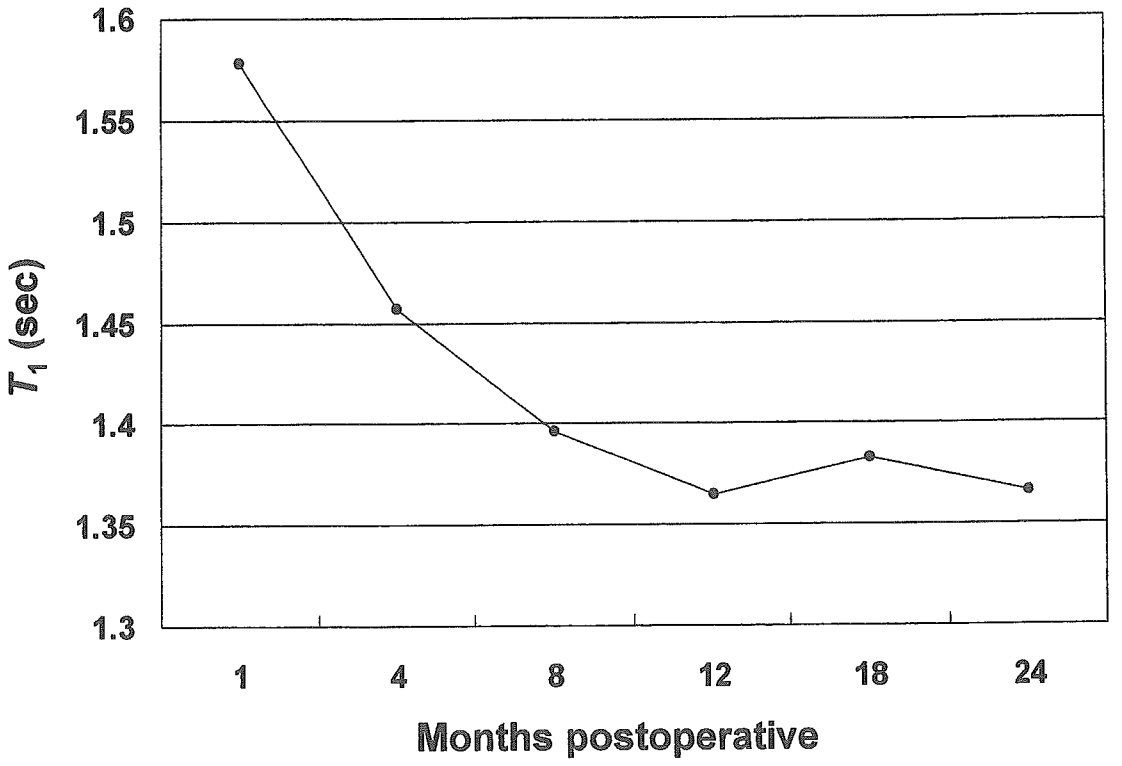

Figure 3. The T_1 in a patient after autologus chondrocytes implantation. The T_1 was at its highest level immediately after ACI, decreased with time to 9 months, and settled to almost level thereafter, which was compatible with the change of SI index.

reported to be generally superior to that after the conventional cartilage repair methods such as subchondral drilling (7), abrasion chondroplasty (8), and microfracture (18). However, histology of reparative cartilage after ACI has been reported to be inferior to normal hyaline cartilage, and has been considered to be mixed cartilage composed of hyaline-like cartilage and fibrocartilage (2,12,16). Our MR imaging findings and histological and biochemical examinations showed reparative cartilage that is definitely inferior to normal hyaline cartilage. This finding was consistent with previously reported findings. This study had a relatively small number of patients and thus statistical analysis concerning the relationship between the histology of biopsy samples and the SI indexes has not been determined. Further studies are required.

ACI is often performed in relatively young patients. Therefore, to avoid long-term degenerative changes, regeneration using more durable hyaline cartilage is desired. To improve ACI to obtain stable clinical results and good long-term outcomes, various studies targeting the acquisition of good repair cartilage tissues close to healthy hyaline cartilage are being performed (5). For the clinical application of these new ACI techniques in the future, our evaluation method using MR imaging may be useful for comparing the maturation process and long-term durability of reparative cartilage between the present and new ACI techniques. Our MR imaging method may be also useful for follow-up on each patient after ACI, but studies on additional cases are necessary.

REFERENCES

1. Breinan, H. A.; Minas, T.; Hsu, H. P.; Nehrer, S.; Shortkroff, S.; Spector, M. Autologous chondrocyte implantation in a canine model: Change in composition of reparative tissue with time. J. Orthop. Res. 19:482–492; 2001.
2. Briggs, T. W.; Mahroof, S.; David, L. A.; Flannelly, J.; Pringle, J.; Bayliss, M. Histological evaluation of chondral defects after autologous chondrocyte implantation of the knee. J. Bone Joint Surg. Br. 85:1077–1083; 2003.
3. Brittberg, M.; Lindahl, A.; Nilsson, A.; Ohlsson, C.; Isaksson, O.; Peterson, L. Treatment of deep cartilage defects in the knee with autologous chondrocyte transplantation. N. Engl. J. Med. 331:889–895; 1994.
4. Brittberg, M.; Nilsson, A.; Lindahl, A.; Ohlsson, C.; Peterson, L. Rabbit articular cartilage defects treated with autologous cultured chondrocytes. Clin. Orthop. 326:270–283; 1996.
5. Brittberg, M.; Tallheden, T.; Sjogren-Jansson, B.; Lindahl, A.; Peterson, L. Autologous chondrocytes used for articular cartilage repair: An update. Clin. Orthop. 391:S337–348; 2001.
6. Disler, D. G. Fat-suppressed three-dimensional spoiled gradient-recalled MR imaging: Assessment of articular and physeal hyaline cartilage. AJR Am. J. Roentgenol. 169:1117–1123; 1997.
7. Dzioba, R. B. The classification and treatment of acute articular cartilage lesions. Arthroscopy 4:72–80; 1988.

8. Friedman, M. J.; Berasi, C. C.; Fox, J. M.; Del Pizzo, W.; Snyder, S. J.; Ferkel, R. D. Preliminary results with abrasion arthroplasty in the osteoarthritic knee. Clin. Orthop. 182:200–205; 1984.
9. Fullerton, G. D. Physiologic basis for magnetic relaxation. In: Stark, D. D.; Bradley, W. G.; eds. Magnetic resonance imaging. St. Louis: Mosby Year Book; 1992:88–108.
10. Gillis, A.; Bashir, A.; McKeon, B.; Scheller, A.; Gray, M. L.; Burstein, D. Magnetic resonance imaging of relative glycosaminoglycan distribution in patients with autologous chondrocyte transplants. Invest. Radiol. 36:743–748; 2001.
11. Henderson, I. J.; Tuy, B.; Connell, D.; Oakes, B.; Hettwer, W. H. Prospective clinical study of autologous chondrocyte implantation and correlation with MRI at three and 12 months. J. Bone Joint Surg. Br. 85:1060–1066; 2003.
12. Horas, U.; Pelinkovic, D.; Herr, G.; Aigner, T.; Schnettler, R. Autologous chondrocyte implantation and osteochondral cylinder transplantation in cartilage repair of the knee joint. A prospective, comparative trial. J. Bone Joint Surg. Am. 85-A:185–192; 2003.
13. Lysholm, J.; Gillquist, J. Evaluation of knee ligament surgery results with special emphasis on use of a scoring scale. Am. J. Sports Med. 10:150–154; 1982.
14. Mainil-Varlet, P.; Aigner, T.; Brittberg, M.; Bullough, P.; Hollander, A.; Hunziker, E.; Kandel, R.; Nehrer, S.; Pritzker, K.; Roberts, S.; Stauffer, E. Histological assessment of cartilage repair: A report by the Histology Endpoint Committee of the International Cartilage Repair Society (ICRS). J. Bone Joint Surg. Am. 85-A(Suppl. 2):45–57; 2003.
15. Peterson, L.; Minas, T.; Brittberg, M.; Nilsson, A.; Sjogren-Jansson, E.; Lindahl, A. Two- to 9-year outcome after autologous chondrocyte transplantation of the knee. Clin. Orthop. 374:212–234; 2000.
16. Richardson, J. B.; Caterson, B.; Evans, E. H.; Ashton, B. A.; Roberts, S. Repair of human articular cartilage after implantation of autologous chondrocytes. J. Bone Joint Surg Br. 81:1064–1068; 1999.
17. Roberts, S.; McCall, I. W.; Darby, A. J.; Menage, J.; Evans, H.; Harrison, P. E.; Richardson, J. B. Autologous chondrocyte implantation for cartilage repair: Monitoring its success by magnetic resonance imaging and histology. Arthritis Res. Ther. 5:60–73; 2003.
18. Rodrigo, J. J.; Steadman, J. R.; Silliman, J. F.; Fulstone, A. H. Improvement of full-thickness chondral defect healing in the human knee after debriedment and microfracture using continuous passive motion. Am. J. Knee Surg. 7:109–116; 1994.

0013-7227/05/$15.00/0
Printed in U.S.A.

Endocrinology 146(6):2620–2628

doi: 10.1210/en.2004-1511

Insulin Receptor Substrate-1 Is Required for Bone Anabolic Function of Parathyroid Hormone in Mice

Masayuki Yamaguchi,* Naoshi Ogata, Yusuke Shinoda, Toru Akune, Satoru Kamekura, Yasuo Terauchi, Takashi Kadowaki, Kazuto Hoshi, Ung-Il Chung, Kozo Nakamura, and Hiroshi Kawaguchi

Departments of Sensory and Motor System Medicine (M.Y., N.O., Y.S., T.A., S.K., K.H., U.-I.C., K.N., H.K.) and Metabolic Diseases (Y.T., T.K.), Faculty of Medicine, University of Tokyo, Tokyo 113-8655, Japan

Bone anabolic action of PTH has been suggested to be mediated by induction of IGF-I in osteoblasts; however, little is known about the molecular mechanism by which IGF-I leads to bone formation under the PTH stimulation. This study initially confirmed in mouse osteoblast cultures that PTH treatment increased IGF-I mRNA and protein levels and alkaline phosphatase activity, which were accompanied by phosphorylations of IGF-I receptor, insulin receptor substrate (IRS)-1 and IRS-2, essential adaptor molecules for the IGF-I signaling. To learn the involvement of IRS-1 and IRS-2 in the bone anabolic action of PTH *in vivo*, *IRS-1*−/− and *IRS-2*−/− mice and their respective wild-type littermates were given daily injections of PTH (80 μg/kg) or vehicle for 4 wk. In the wild-type mice, the PTH injection increased bone mineral densities of the femur, tibia, and vertebrae by 10–20% without altering the serum IGF-I level. These stimulations were similarly seen in *IRS-2*−/− mice; however, they were markedly suppressed in *IRS-1*−/− mice. Although the PTH anabolic effects were stronger on trabecular bones than on cortical bones, the stimulations on both bones were blocked in *IRS-1*−/− mice but not in *IRS-2*−/− mice. Histomorphometric and biochemical analyses showed an increased bone turnover by PTH, which was also blunted by the IRS-1 deficiency, though not by the IRS-2 deficiency. These results indicate that the PTH bone anabolic action is mediated by the activation of IRS-1, but not IRS-2, as a downstream signaling of IGF-I that acts locally as an autocrine/paracrine factor. (*Endocrinology* 146: 2620–2628, 2005)

ANABOLIC EFFECTS of PTH on bone have attracted considerable clinical attention and led to the approval of PTH for osteoporosis treatment (1–3). Although it has been well established that intermittent administration of PTH exerts potent anabolic effects on bone in animals and humans (4), the underlying mechanism is still controversial and unclear. PTH is reported to increase production of osteoprogenitors and differentiation of osteoblasts from an existing pool of osteoprogenitors and to decrease apoptosis of preexisting osteoblasts (5–7). Accumulated evidence has shown that IGF-I is an attractive candidate as a mediator for some or all of the anabolic actions of PTH on bone, in that PTH stimulates IGF-I production by osteoblastic cells (8, 9) and IGF-1 can reproduce the effects of PTH on osteoblast proliferation, differentiation, and survival (10). From *in vitro* studies, IGF-I-blocking antibodies inhibited collagen synthesis and alkaline phosphatase (ALP) activity, as well as the expression of osteocalcin mRNA induced by PTH stimulation on osteoblasts (11, 12). Furthermore, PTH anabolic actions were suppressed when administered to IGF-I-deficient mice (13, 14), suggesting the importance of the IGF-I signaling *in vivo*.

IGF-I initiates cellular responses by binding to its cell-surface receptor tyrosine kinase IGF-I receptor, which then activates essential adaptor molecule insulin receptor substrates (IRS's) followed by downstream signaling pathways like phosphatidylinositol-3 kinase (PI3K)/Akt and MAPKs (15). The mammalian IRS family contains at least four members: ubiquitous IRS-1 and IRS-2, adipose tissue-predominant IRS-3, and IRS-4 which is expressed in the thymus, brain, and kidney. We previously reported that IRS-1 and IRS-2 are expressed in bone (16, 17). Our further studies on mice lacking the IRS-1 gene (*IRS-1*−/− mice) or the IRS-2 gene (*IRS-2*−/− mice) revealed that these knockout mice exhibited severe osteopenia with distinct mechanisms: *IRS-1*−/− mice showed a low bone turnover in which both bone formation and resorption were decreased (16), whereas *IRS-2*−/− mice showed an uncoupling status with decreased bone formation and increased bone resorption (17). It therefore seems that under physiological conditions, IRS-1 is important for maintaining bone turnover, whereas IRS-2 is important for retaining the predominance of anabolic function over catabolic function of osteoblasts.

To learn the molecular mechanism by which IGF-I leads to bone formation under the PTH stimulation, the present study investigated the role of IRS-1 and IRS-2 in mediating the anabolic effects of recombinant human PTH(1–34) on bone. We first studied the effects of PTH on the IGF-I related molecules in cultured mouse osteoblasts and examined skeletal responses to PTH in *IRS-1*−/− and *IRS-2*−/− mice.

First Published Online February 17, 2005

* Dr. Yamaguchi is deceased. Regrettably, Masayuki Yamaguchi died at much too young an age and before the publication of this paper. We dedicate this paper to him and to his family.

Abbreviations: ALP, Alkaline phosphatase; BMD, bone mineral density; GAPDH, glyceraldehyde-3-phosphate dehydrogenase; GMA, glycolmethacrylate; IRS, insulin receptor substrate; PI3K, phosphatidylinositol-3 kinase; PKA, protein kinase A; pQCT, peripheral quantitative computerized tomography; WT, wild type.

Endocrinology **is published monthly by The Endocrine Society (http://www.endo-society.org), the foremost professional society serving the endocrine community.**

Materials and Methods

Animals

Mice with the original C57BL6/CBA hybrid background were generated and maintained as reported previously (16, 17). In each experiment, homozygous wild-type (WT) and *IRS-1*−/− male mice, as well as homozygous WT and *IRS-2*−/− male mice, that were littermates generated from the intercross between heterozygous mice were compared. All mice were kept in plastic cages under standard laboratory conditions with a 12-h dark, 12-h light cycle, a constant temperature of 23 C, and humidity of 48%. The mice were fed a standard rodent diet (CE-2; CLEA Japan, Inc., Tokyo, Japan) containing 25.2% protein, 4.6% fat, 4.4% fiber, 6.5% ash, 3.44 kcal/g, 2.5 IU vitamin D_3/g, 1.09% calcium, and 0.93% phosphorus with water *ad libitum*. All animal experiments were reviewed and approved by the University of Tokyo, Faculty of Medical Animal Care and Use Committee, before the study.

Osteoblast cultures

Osteoblasts were isolated from calvariae of neonatal WT, *IRS-1*−/−, and *IRS-2*−/− littermates. Calvariae were digested for 10 min, 5 times, at 37 C in an enzyme solution containing 0.1% collagenase and 0.2% dispase. Cells isolated by the last four digestions were combined as an osteoblast population and cultured in αMEM (Invitrogen, Carlsbad, CA) containing 10% FBS (HyClone Laboratories, Inc., Logan, UT) and 50 μg/ml ascorbic acid (Sigma-Aldrich Corp., St. Louis, MO).

For real-time quantitative RT-PCR analysis, primary osteoblasts were inoculated at a density of 1×10^4 cells/well in a 24-multiwell plate, and cultured in the medium above, with or without 100 nM recombinant human PTH(1–34) (Sigma-Aldrich Corp.) for 14 d. Total RNA was extracted with an ISOGEN kit (Wako Pure Chemical Industries Ltd., Osaka, Japan), according to the manufacturer's instructions. One microgram of RNA was reverse-transcribed using a Takara RNA PCR Kit, version 2.1 (Takara Shuzo Co., Shiga, Japan), to make single-stranded cDNA. The ABI Prism Sequence Detection System 7000 and Primer Express Software (Applied Biosystems, Foster City, CA) were used for PCR amplification and quantitative analysis, respectively. For the IGF-I gene, a set of primers was designed using sequences obtained from the GenBank as follows: 5′GACAGATACARRCTGTGCTCA-3′ and 5′-CTGAAGCTTGCTAACATCGC-3′. The PCR consisted of QuantiTect SYBR Green Master Mix (QIAGEN, Tokyo, Japan), 0.3 μM specific primers, and 20 ng cDNA.

For the IGF-I protein level measurement, primary osteoblasts were cultured, as described above, for 14 d, and the free IGF-I concentration in the culture media was measured with a Non-Extraction IGF-I ELISA kit (Diagnostic Systems Laboratories, Inc., Sparks, MD).

For ALP activity measurement, primary osteoblasts were cultured in the medium above with or without 10 ng/ml recombinant mouse IGF-I (Sigma-Aldrich Corp.) and 5 nM antimouse IGF-I antibody (Sigma-Aldrich Corp.). At 14 d of culture, cells were sonicated in 10 mM Tris-HCl buffer (pH 8.0) containing 1 mM $MgCl_2$ and 0.5% Triton X-100, and ALP activity in the lysate was measured using an ALP assay kit (Wako Pure Chemical Industries Ltd.). The protein content was determined using BCA protein assay reagent (Pierce Chemical Co., Rockford, IL).

Immunoprecipitation and immunoblotting

After stimulation by 100 nM PTH for the indicated time, cultured osteoblasts were lysed with TNE buffer (10 mM Tris-HCl, 150 mM NaCl, 1% NP-40, 1 mM EDTA, 10 mM NaF, 2 mM Na_3VO_4, 1 mM aminoethylbenzenesulfonyl fluoride, and 10 μg/ml aprotinin). A part of the cell lysates (100 μg) was immunoprecipitated with an antiphosphotyrosine antibody, an antimouse IGF-I receptor antibody, an antimouse insulin receptor antibody, an antimouse IRS-1 antibody, or an antimouse IRS-2 antibody (all from Upstate Biotechnology, Inc., Waltham, MA) conjugated to protein G-Sepharose (Invitrogen) for 4 h at 4 C. The cell lysates with or without the immunoprecipitation that contained an equivalent amount of protein (20 μg) were electrophoresed by 8% SDS-PAGE and transferred to nitrocellulose membrane. After blocking with 5% BSA solution, they were incubated with the antibodies above, and the immunoreactive bands were stained using the ECL chemiluminescence reaction (Amersham, Arlington Heights, IL). The intensity of each band was measured by densitometry (Bio-Rad Laboratories, Inc., Richmond, CA) and was expressed as the mean value of five independent experiments.

PTH treatment on mice

IRS-1−/− mice and their littermates and *IRS-2*−/− mice and their littermates (males, all n = 10) received either PTH (80 μg/kg body weight) or vehicle (PBS) by sc injection every day for 4 wk beginning at 10 wk of age. Blood samples were collected by heart puncture under nembutal (Dainippon Pharmaceutical Co., Ltd., Osaka, Japan) anesthesia before being killed. For radiological and histological analyses, animals were killed after 4 wk of PTH treatment by diethylether. The right femurs and tibiae were obtained for bone densitometry, and the left femurs and tibiae for peripheral quantitative computerized tomography (pQCT) and histological analyses, respectively. Lumbar vertebral bodies from L2–L5 were also obtained for bone densitometry.

Bone densitometry and pQCT

Bone mineral density (BMD; milligrams per square centimeter) of the right femur, tibiae, and L2–L5 vertebral bodies was determined using dual-energy x-ray absorptiometry (PIXImus Mouse Densitometer; Lunar Corp., Madison, WI) according to the manufacturer's instructions. Computerized tomography was performed with a pQCT analyzer (XCT Research SA+; Stratec Medizintechnik GmbH, Pforzheim, Germany) operating at a resolution of 80 μm. Metaphyseal pQCT scans of the left femurs were performed to measure the trabecular volumetric BMD. The scan was positioned in the metaphysis at 1.2 mm proximal from the distal growth plate. Because this area contains trabecular and cortical bones, the trabecular bone region was defined by setting the threshold to 395 mg/cm^3. Middiaphyseal pQCT scans of the left femurs were performed to determine the cortical thickness. The middiaphyseal region of femurs in mice contains mostly cortical bone. The cortical bone region was defined by setting the threshold to 690 mg/cm^3. The interassay coefficients of variation for the pQCT measurements were less than 2%.

Histological analyses

For the assessment of dynamic histomorphometric indices, mice were injected with calcein (16 mg/kg body weight) sc at 10 d and 3 d before being killed, after which the left tibiae were excised and fixed with ethanol, and the undecalcified bones were embedded in glycolmethacrylate. Three-micrometer sagittal sections from the proximal parts of tibiae were stained with toluidine blue and were visualized under fluorescent light microscopy for calcein labeling. The specimens were subjected to histomorphometric analyses using a semiautomated system (Osteoplan II; Carl Zeiss, Oberkochen, Germany), and measurements were made at ×400 magnification. Parameters for the trabecular bone were measured in an area 1.2 mm in length, from 250 μm below the growth plate at the proximal metaphysis of the tibiae. Nomenclature, symbols, and units are those recommended by the Nomenclature Committee of the American Society for Bone and Mineral Research (18).

Serum biochemical assays

For serum IGF-I levels, acid ethanol extraction was used to remove the IGF-binding proteins, and the extracted samples were assayed for IGF-I with a RIA kit from Nichols Institute Diagnostics (San Juan Capistrano, CA). Serum osteocalcin levels were determined by using the competitive RIA kit (Biomedical Technologies, Stoughton, MA). The sensitivity of the assay was 19 ng/ml, and the interassay and intraassay coefficients of variation were less than 10%. Serum ALP activity was determined by liquitech ALP kit (Roche Diagnostics, Basel, Switzerland) with an autoanalyzer (type 7170; Hitachi High-Technologies Corporation, Tokyo, Japan). ALP activity of the blood samples was expressed as nanomoles per minute and per milligram of protein.

Statistical analysis

Means of groups were compared by ANOVA, and significance of differences was determined by *post hoc* testing using Bonferroni's method.

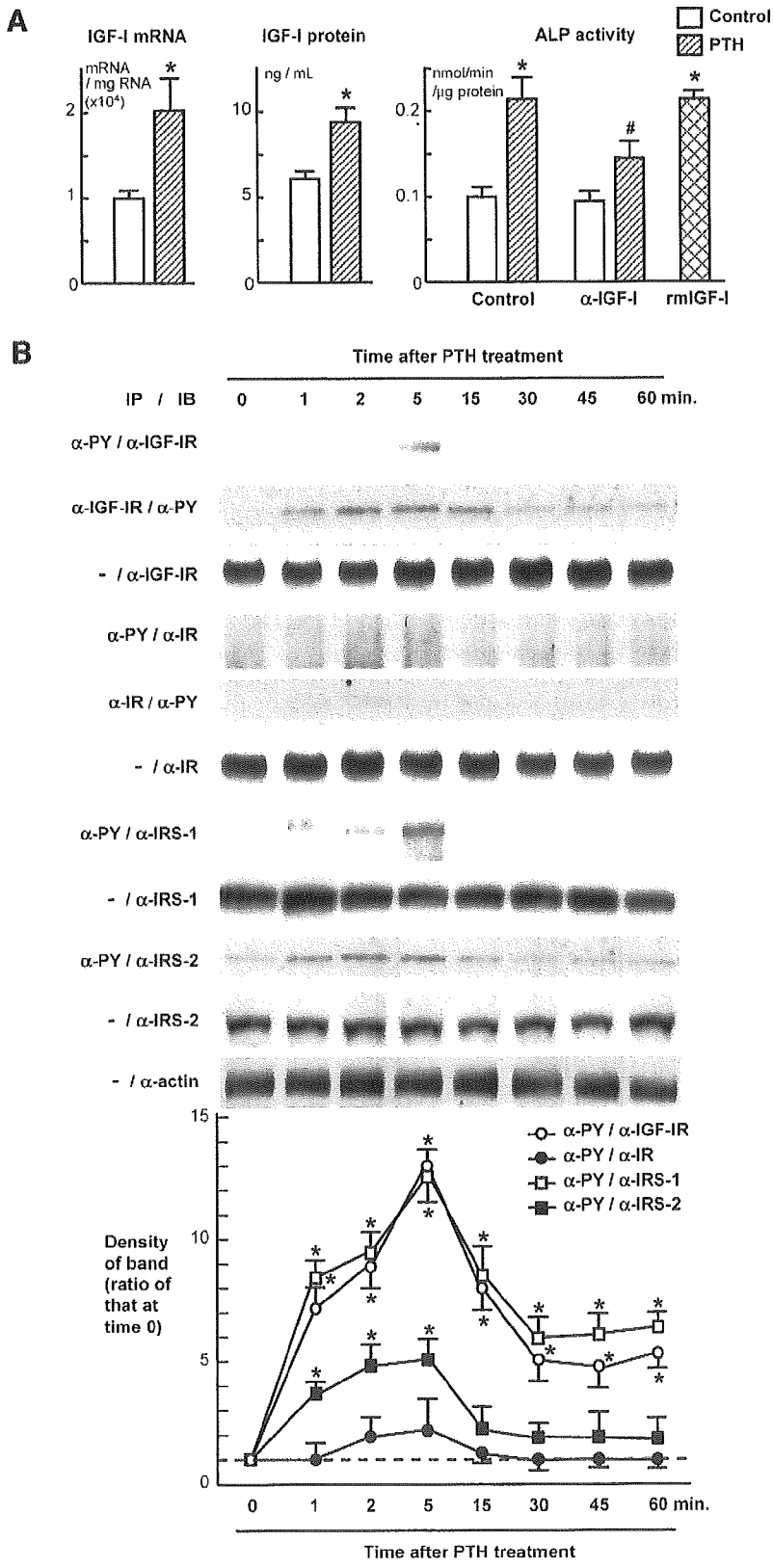

FIG. 1. Effects of PTH on cultured osteoblasts isolated from neonatal mouse calvariae. A, IGF-I mRNA level determined by real-time quantitative RT-PCR (*left*), IGF-I protein level in the culture medium (*middle*), and ALP activity in the cell lysate (*right*) in the primary calvarial osteoblast culture in the presence and absence of PTH (100 nM), an antibody against IGF-I (α-IGF-I, 5 nM), and recombinant mouse IGF-I (rmIGF-I, 10 ng/ml) for 2 wk. Data are expressed as means (*bars*) ± SEM (*error bars*) for eight wells per group. *, Significant increase compared with the control culture, $P < 0.01$; #, significant inhibition by α-IGF-I, $P < 0.05$. B, Protein levels by immunoprecipitation (IP) and immunoblotting (IB) of IGF-I receptor, insulin receptor, IRS-1, and IRS-2 with or without phosphorylation in osteoblasts cultured with PTH (100 nM) for the indicated times. Some of the cell lysates were immunoprecipitated with an antiphosphotyrosine antibody (α-PY), and the cell lysates with or without (−) the immunoprecipitation were immunoblotted with an antimouse IGF-I receptor (α-IGF-IR), an antimouse insulin receptor (α-IR), an antimouse IRS-1 (α-IRS-1), or an antimouse IRS-2 antibody (α-IRS-2). Some of the cell lysates were reciprocally immunoprecipitated with α-IGFR or α-IR and immunoblotted with α-PY. Blottings with an anti-β-actin (α-actin) were used as loading controls. Similar results were obtained in five independent experiments. The graph below shows the mean values of the band intensities of phosphorylated proteins normalized to α-actin quantified using densitometry in five independent experiments. Data are expressed as the ratio of the value at time zero. Although the data of proteins without phosphorylation are not shown in the graph, they were not significantly affected by PTH during the observation period (the ratio values were from 0.8–1.2). Data are expressed as means (*bars*) ± SEM (*error bars*) of five independent experiments. *, Significant difference from that at time zero, $P < 0.01$.

Results

Effects of PTH on cultured osteoblasts

We first examined the effects of recombinant human PTH(1–34) in the cultures of primary osteoblasts derived from mouse calvariae. IGF-I mRNA level determined by real-time RT-PCR, IGF-I protein level in the cultured medium, and ALP activity in the cell lysate were all increased about 2-fold with PTH (100 nM) treatment compared with the control cultures (Fig. 1A). A neutralizing antibody against IGF-I significantly, although not completely, suppressed the PTH stimulation of ALP activity. Furthermore, addition of a recombinant mouse IGF-1 at a concentration similar to that of endogenous IGF-I (10 mg/ml) stimulated by PTH increased the ALP activity to a level similar to that by PTH. These lines of results confirm that the PTH anabolic action is, at least partly, mediated by the IGF-I production in osteoblasts, as previously reported (8, 11, 12).

To provide some insights into signaling pathways that are involved in the PTH action on primary osteoblasts, we examined the phosphorylations of IGF-I receptor, insulin receptor, IRS-1, and IRS-2 in five independent experiments (Fig. 1B). Immunoprecipitation and immunoblotting analyses revealed that phosphorylations of IGF-I receptor and IRS-1 were clearly induced at 1 min and reached maximum at 5 min. IRS-2 was also phosphorylated by PTH, although not as strongly as IGF-I receptor and IRS-1. Insulin receptor was hardly phosphorylated by PTH. None of the protein levels of IGF-I receptor, insulin receptor, IRS-1, or IRS-2 were altered by PTH during the observation period up to 60 min, suggesting that PTH does not show transcriptional or translational regulation of these signaling molecules. These results indicate that IGF-I production followed by the activation of its intracellular signaling pathways may be related to the PTH action in osteoblasts.

Effects of PTH on bones in IRS-1−/− and IRS-2−/− mice

To learn the roles of the IRS-1 and IRS-2 in the PTH action on bone *in vivo*, we analyzed the PTH effects on the knockout mice by comparing them with those of respective WT littermates using radiological and histological analyses. Both knockout mice were healthy, with no abnormality in major organs except that *IRS-1−/−* mice alone showed about 20% shorter limbs and trunk, whereas *IRS-2−/−* mice were normal in size compared with WT littermates (19–21). The mice (10 wk old, males) were given daily sc injections of PTH (80 μg/kg) or vehicle for 4 wk, after which their femurs, tibiae, and lumbar vertebrae underwent radiological and histological analyses. As we previously reported for bone phenotypes under physiological conditions (16, 17), both knockout mice showed osteopenia when injected with vehicle: BMDs of femur, tibia, and lumbar vertebra in *IRS-1−/−* and those of femur and tibia in *IRS-2−/−* were significantly lower than respective WT littermates (Fig. 2). The PTH injection increased BMDs of these bones 10–20% in WT; however, this increase was hardly seen in the *IRS-1−/−* bones (Fig. 2A). The stimulations by PTH, on the contrary, seen in the *IRS-*

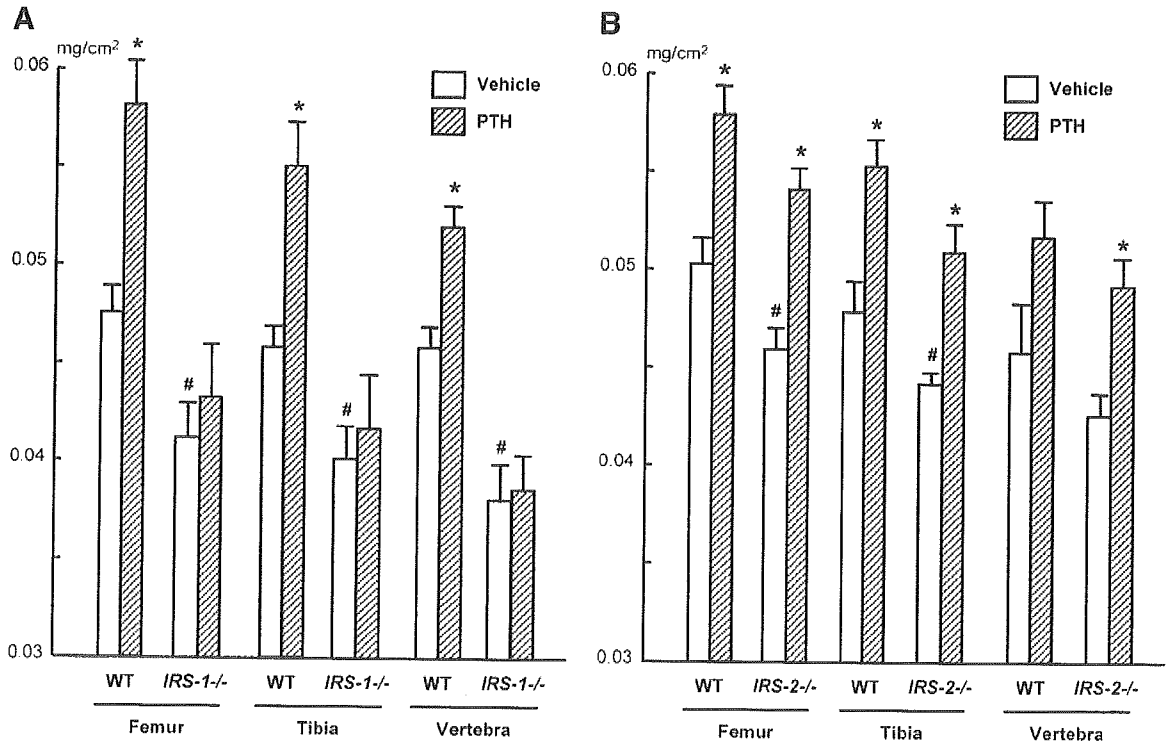

FIG. 2. Effects of PTH treatment on bone densities in *IRS-1−/−* mice (A) and *IRS-2−/−* mice (B), compared with respective WT littermates. *IRS-1−/−* mice and the littermates and *IRS-2−/−* mice and the littermates (males, 10 wk old, n = 10/group) received daily sc injections of either PTH (80 μg/kg body weight) or vehicle for 4 wk. Mice were killed; and the right femurs, tibiae, and L2–L5 vertebral bodies were excised. BMD values of the entire femurs, tibiae, and vertebral bodies were determined using dual-energy x-ray absorptiometry. Data are expressed as means (*bars*) ± SEM (*error bars*) of 10 bones per group. *, Significant effect of PTH, $P < 0.01$; #, significant difference from WT, $P < 0.01$.

2−/− bones were similar to those of the WT littermates (Fig. 2B). These results suggest that IRS-1, but not IRS-2, is needed for the bone anabolic action of PTH.

We further examined trabecular and cortical bones separately in the femurs using pQCT (Fig. 3). In trabecular bones at the distal metaphysis of femurs, both *IRS-1*−/− and *IRS-2*−/− mice showed lower bone density (Fig. 3, A and C). PTH injection increased the trabecular bone density about 60% in WT. Here again, this PTH effect was abolished by the IRS-1 deficiency but was not altered by the IRS-2 deficiency. In the cortical bones at the midshaft of the femurs, although the PTH effects on cortical thickness were milder than those on the trabecular density, this was blocked by the IRS-1 deficiency, although not by the IRS-2 deficiency (Fig. 3, B and D).

Histological features of the proximal tibiae showed decreases of trabecular bones in vehicle-treated *IRS-1*−/− and *IRS-2*−/− mice compared with the respective WT littermates (Fig. 4). After PTH treatment for 4 wk, increases of these bones were observed in *IRS-2*−/− and WT littermates to a similar extent (Fig. 4B), whereas no increase was observed in the *IRS-1*−/− trabeculae (Fig. 4A). Bone histomorphometric measurements in this area confirmed that the PTH injection augmented the bone volume (trabecular bone volume expressed as a percent of total tissue volume) of WT mice by 50–60%, with the increases of both bone formation parameters (percent of bone surface covered by cuboidal osteoclasts, and bone formation rate) and resorption parameters (percent of bone surface covered by mature osteoclasts, and percent of eroded surface), indicating a high bone turnover

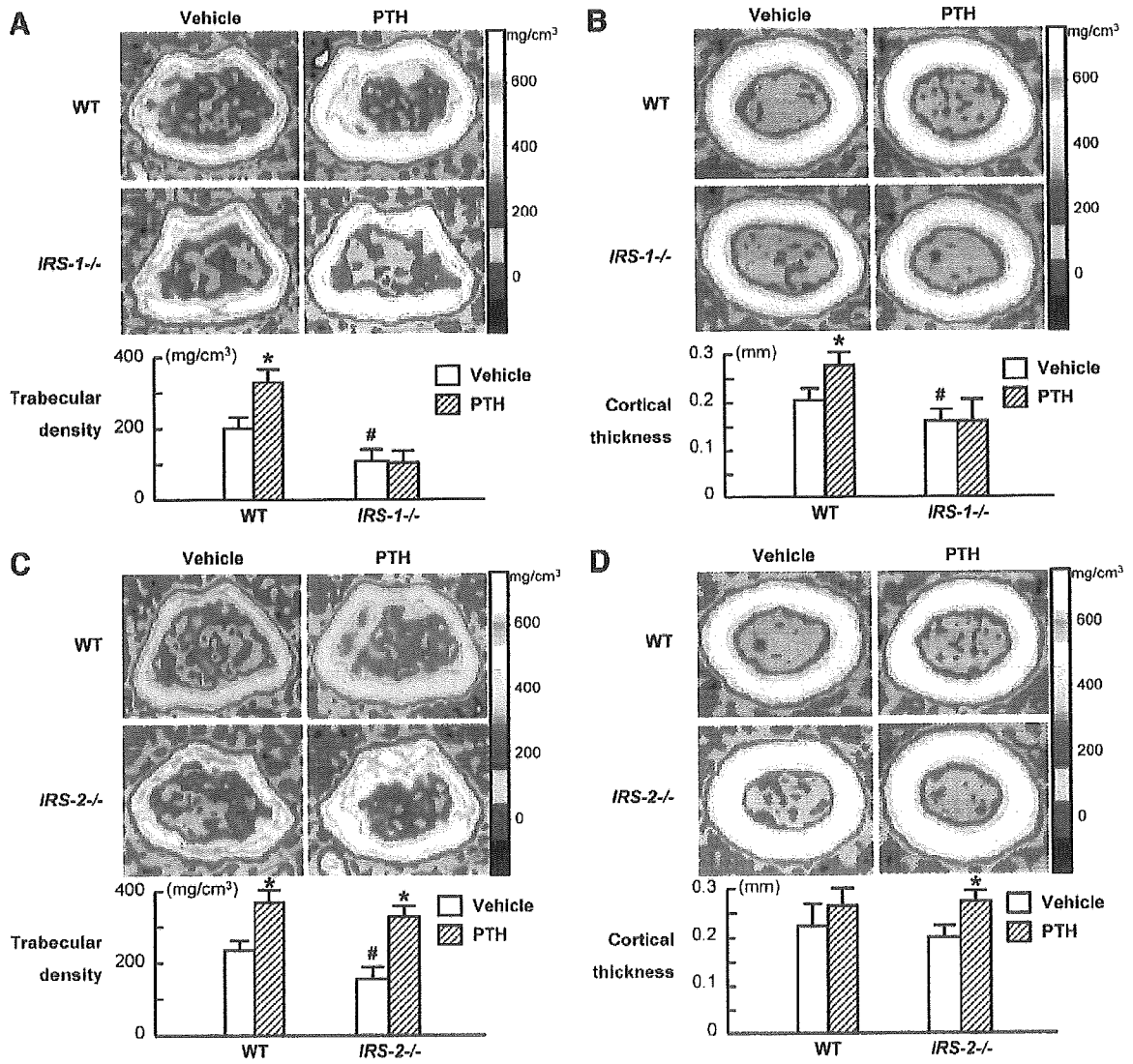

FIG. 3. Effects of PTH treatment on trabecular and cortical bones in *IRS-1*−/− mice (A and B) and *IRS-2*−/− mice (C and D), compared with respective WT littermates. After daily injections of either PTH (80 μg/kg body weight) or vehicle for 4 wk, mice were killed, and the distal metaphysis (A and C) and the middiaphysis (B and D) of the excised left femurs underwent pQCT analysis. The color gradient indicating bone density is shown in the *right bars*. The trabecular density at the metaphysis and the cortical thickness at the middiaphysis are shown in the graphs *below*. Data in all graphs are expressed as means (*bars*) ± SEMs (*error bars*) of 10 bones per group. *, Significant effect of PTH, $P < 0.01$; #, significant difference from WT, $P < 0.01$.

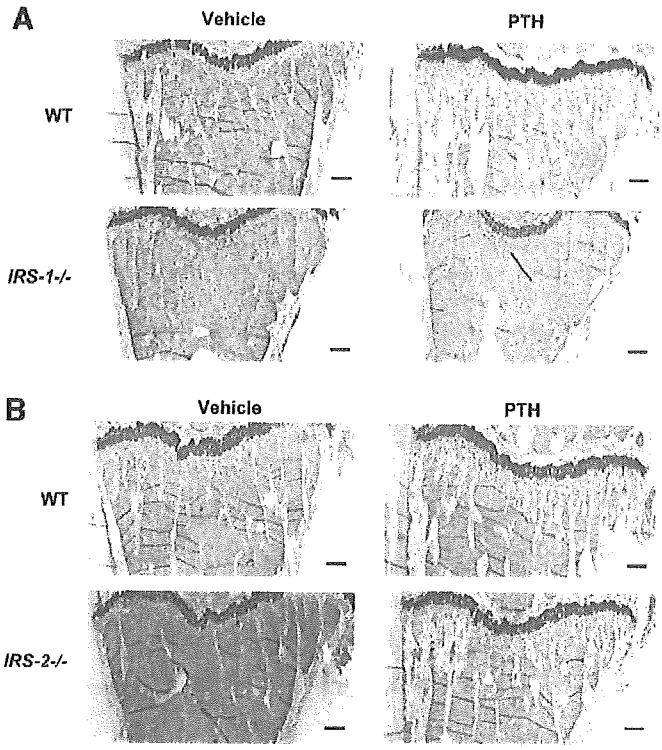

FIG. 4. Effects of PTH treatment on histological features of the proximal metaphysis of tibiae in *IRS-1−/−* mice (A) and *IRS-2−/−* mice (B), compared with respective WT littermates. After death, the left tibiae were excised, fixed, and embedded in GMA without decalcification, and the sagittal sections were stained by toluidine blue. Representative samples are shown from mice of each genotype given either PTH or vehicle. Data of histomorphometric analyses are shown in Table 1. *Bar*, 100 μm.

state (Table 1). *IRS-1−/−* and *IRS-2−/−* mice showed 30–40% lower bone volume than respective WT littermates when injected with vehicle. As we previously reported (16, 17), *IRS-1−/−* exhibited a low bone turnover, with decreases in both bone formation and resorption parameters, whereas *IRS-2−/−* mice showed an uncoupling status of bone turnover, with decreased bone formation and increased bone resorption. The PTH injection affected neither the bone volume nor the bone turnover in the *IRS-1−/−* mice; however, in the *IRS-2−/−* mice, PTH increased bone volume mainly through the up-regulation of bone formation rather than bone resorption.

Effects of PTH on blood chemistries in IRS-1−/− and IRS-2−/− mice

The serum markers osteocalcin and ALP supported the increase of bone formation by the PTH injection in WT mice (Fig. 5). Here again, these stimulations were not seen in *IRS-1−/−* mice but were maintained in *IRS-2−/−* mice. Because the serum IGF-I levels were not different between PTH- and vehicle-treated mice in all genotypes, IGF-I that is induced by PTH, as shown in Fig. 1A, seemed not to act as a systemic factor but to act locally in bone as an autocrine/paracrine factor.

Discussion

The present study demonstrated that the bone anabolic function of PTH is mediated by the activation of IGF-1R and IRS-1, but not IRS-2, as a downstream signaling of IGF-I that acts locally in bone. Although IRS-1 and IRS-2 are known to be essential for intracellular signaling of IGF-I and insulin, these two adaptor molecules have distinct biological roles and are differentially expressed in a variety of cells. Regarding glucose homeostasis, IRS-1 plays an important role in the metabolic actions of insulin, mainly in skeletal muscle and adipose tissue, whereas IRS-2 does so in the liver (22). Our previous studies revealed that only IRS-1, but not IRS-2, was expressed in the cartilage of the growth plate or the fracture callus, so that skeletal growth and fracture healing were impaired in *IRS-1−/−* mice, whereas they were normal in *IRS-2−/−* mice (21, 23). In bone, IRS-1 is expressed solely in cells of osteoblast lineage, whereas IRS-2 is expressed in cells of both osteoblast and osteoclast lineages (16, 17). As described above, our previous studies on bones of these two knockout mice disclosed that IRS-1 is important for maintaining bone turnover, and IRS-2 for maintaining predominance of anabolic function over catabolic function of osteoblasts (16, 17). In the meantime, previous and present studies have shown that PTH treatment increases bone turnover in animals and humans (24, 25). The fact that the suppression of bone turnover by IRS-1 deficiency suppressed the bone anabolic action of PTH suggests the importance of elevated turnover for the PTH function. This is consistent with the

TABLE 1. Histomorphometry of trabecular bones in proximal tibiae

	BV/TV (%)	Ob.S/BS (%)	BFR (mm^3/cm^2/year)	Oc.S/BS (%)	ES/BS (%)
WT + vehicle	9.35 ± 0.69	8.38 ± 0.80	4.96 ± 0.62	5.28 ± 1.39	6.02 ± 0.99
WT + PTH	14.23 ± 1.84[a]	12.27 ± 1.89	8.21 ± 0.83[a]	10.51 ± 1.35[a]	9.14 ± 0.51[a]
IRS-1−/− + vehicle	5.97 ± 0.62[b]	2.67 ± 1.02[b]	1.06 ± 0.29[b]	2.23 ± 0.38[b]	3.42 ± 0.59[b]
IRS-1−/− + PTH	6.25 ± 0.73	4.50 ± 0.93	1.31 ± 0.38	2.71 ± 1.03	4.14 ± 1.22
WT + vehicle	9.94 ± 0.81	8.49 ± 1.53	4.22 ± 0.29	4.90 ± 0.78	5.35 ± 0.71
WT + PTH	15.79 ± 1.60[a]	13.61 ± 2.24	9.72 ± 1.83[a]	8.84 ± 1.27[a]	9.60 ± 1.21[a]
IRS-2−/− + vehicle	6.86 ± 0.63[b]	12.93 ± 2.83	2.06 ± 0.31[b]	7.92 ± 0.69[b]	9.22 ± 1.09[b]
IRS-2−/− + PTH	16.95 ± 2.27[a]	15.71 ± 1.80	8.71 ± 0.59[a]	9.93 ± 1.43	11.42 ± 2.01

Parameters for the trabecular bone were measured in an area 1.2 mm in length from 250 μm below the growth plate at the proximal metaphysis of the tibiae in Villanueva-Goldner and calcein double-labeled sections. Data expressed as means and SEM for 10 bones per group. BV/TV, Trabecular bone volume expressed as a percentage of total tissue volume; Ob.S/BS, percentage of bone surface covered by cuboidal osteoblasts; BFR, bone formation rate; Oc.S/BS, percentage of bone surface covered by mature osteoclasts; ES/BS, percentage of eroded surface.

[a] Significant effect of PTH, $P < 0.01$.

[b] Significant difference from WT, $P < 0.01$.

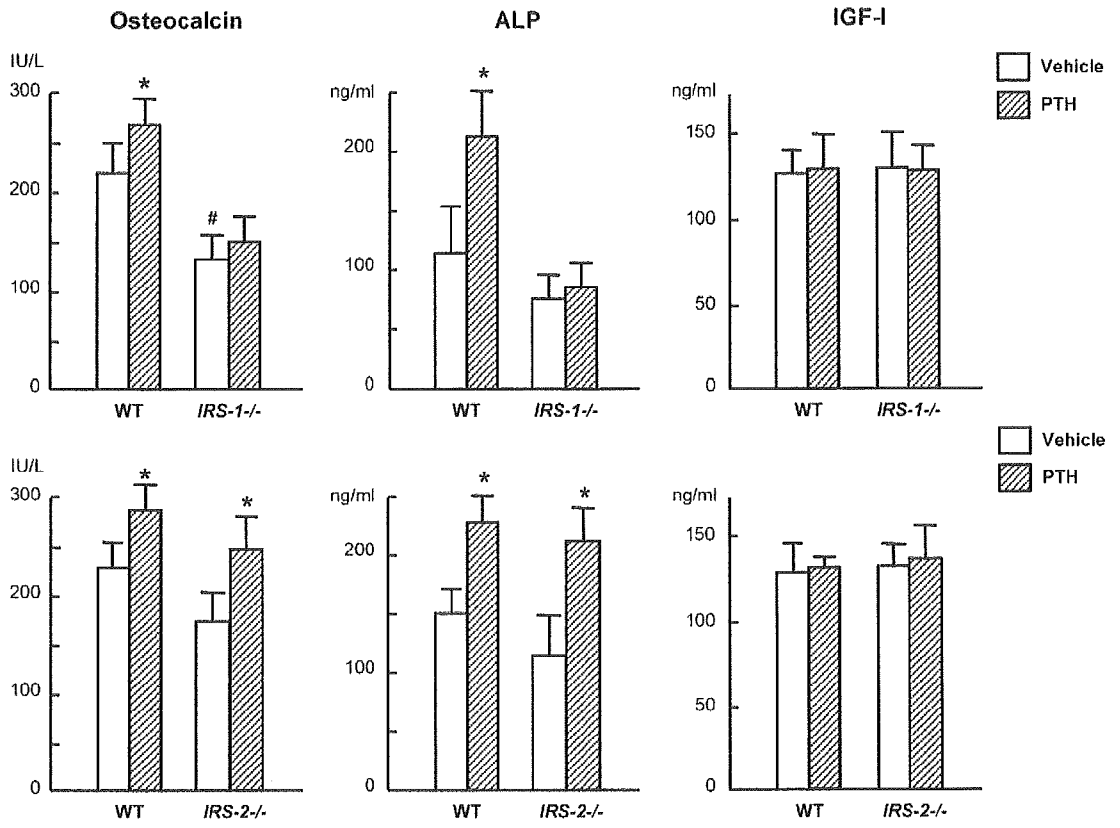

FIG. 5. Effects of PTH treatment on serum osteocalcin, ALP, and IGF-I levels in *IRS-1−/−* mice and *IRS-2−/−* mice, compared with respective WT littermates. Mice received either PTH or vehicle for 4 wk as described above, and blood samples were collected by heart puncture before death. The levels were measured as described in *Materials and Methods*. *, Significant effect of PTH, $P < 0.05$; #, significant difference from WT, $P < 0.05$.

results of clinical studies showing that the concurrent use of alendronate, a potent bisphosphonate that markedly suppresses bone turnover, reduced the bone anabolic action of PTH in male and female osteoporosis patients (26, 27).

Because it is unlikely that PTH directly activates IGF-I receptor and IRS-1, there seem to be two possible molecular mechanisms underlying the suppression of PTH action by the IRS-1 deficiency: 1) PTH induces IGF-I production, causing IGF-I receptor and IRS-1 activation; and 2) IRS-1 signaling affects the intracellular signaling lying downstream of the PTH/PTH-related protein receptor after PTH binds to it. The quick phosphorylation of IGF-I receptor and IRS-1 after PTH treatment in primary osteoblast culture in the present study (Fig. 1B) supports the former mechanism. Hormones like PTH and prostaglandin E_2 that increase cAMP synthesis and PKA activation are reported to induce the transcription of IGF-I by way of a C/EBP (CCAAT/enhancer-binding protein)-sensitive element in exon 1 of the IGF-I gene (28, 29). However, the latter possibility cannot be denied, because the inhibition of the PTH stimulation on ALP activity by a neutralizing antibody against IGF-I was not complete, but partial, in the primary osteoblast culture (Fig. 1A). In fact, IRS-1 and PTH/PPR (PTH/PTH-related protein receptor) are known to share several common signaling pathways. The main pathways lying downstream of IRS-1 are PI3K/Akt and MAPKs, which are important regulators of cell growth and differentiation. PTH has been shown to directly activate the p42/p44 MAPK by protein kinase C-dependent, but Ras-independent, signaling in rat osteoblasts (30) and to upregulate PI3K/Akt activity, which contributes to the MAPK activation in rat enterocytes (31). In addition, both PTH and IGF-I have been shown to be involved in the activation of c-*fos* expression (32, 33) and cyclin-dependent kinase expression in osteoblasts (34, 35). These lines of evidence indicate the PTH signaling pathway may possibly be affected by the IRS-1 signaling at several points, and the absence of an IRS-1 signaling pathway may result in the failure of PTH to stimulate key target molecules necessary for its anabolic action.

Another potential explanation for the lack of PTH response in *IRS-1−/−* mice could be the impairment of proliferation or differentiation ability of osteoprogenitor cells, so that they are insensitive not only to PTH but also to other stimulations. In fact, our present and previous studies demonstrated the decreases in histomorphometric parameters and serum markers for bone formation in *IRS-1−/−* mice under physiological conditions (16). In this regard, however, our previous study has shown that proliferation and differentiation of primary calvarial cells were stimulated, responding to fibroblast growth factor-2 and bone morphogenetic protein-2, respectively, similarly to those of the WT cells, indicating that functions of *IRS-1−/−* cells are normal as long as adequate signals other than IGF-I signal were applied (16). Hence, the decreased bone formation under physiological conditions in *IRS-1−/−* mice is likely to be due to the deficit

of anabolic signaling of endogenous IGF-I. Interestingly, PTH increased the IGF-I protein level in the culture medium of primary osteoblasts (Fig. 1A) but did not affect the serum IGF-I level *in vivo* (Fig. 5), indicating the importance of local action of IGF-I as an autocrine/paracrine factor for bone formation rather than its systemic action as a hormone. This result is consistent with previous reports that disruption of IGF-I genes, specifically in liver, decreased serum IGF-I by 80% but caused no skeletal abnormality (36, 37). Because the remaining 20% IGF-I in serum is probably derived from several tissues, including bone, it is not surprising that PTH treatment did not increase circulating levels of IGF-I. The findings that PTH anabolic effects can be suppressed by an IGF-I-neutralizing antibody in osteoblast cultures in the present and previous studies (11, 12) also support the idea that the PTH-induced bone formation involves increased local production, but not increased circulating levels, of IGF-I.

The requirement of IGF-I/IRS-1 for mediating the anabolic effects of bone regulatory hormones may not be unique to PTH, because previous findings have revealed that many of the major hormones exert significant effects on IGF-I expression. GH is a well-known stimulus of IGF-I production in a variety of tissues, including bone, and exerts its effects on bone mainly through IGF-I mediation (38). Estradiol, another important regulator of skeletal metabolism, has been shown to increase IGF-I production, and IGF-I receptor-blocking antibodies inhibited the proliferative effect of estradiol in rat osteoblasts (39, 40). Similarly, other hormones with potent effects on bone, such as thyroid hormone and androgens, alter IGF-I levels in bone in a manner consistent with IGF-I playing a role in the actions of these hormones on bone (41, 42). Although these studies did not examine the involvement of IRS-1 or IRS-2 in their anabolic actions, it is possible that the IGF/IRS pathway might be a common signaling for actions of these major hormones in bone. Further understanding of the molecular mechanism by which the hormones induce IGF-I and the intracellular signaling that lies downstream of IGF-I/IRS in osteoblasts will greatly help to elucidate the complex network of bone formation under systemic regulations.

Acknowledgments

Received November 22, 2004. Accepted February 4, 2005.

Address all correspondence and requests for reprints to: Hiroshi Kawaguchi, M.D., Ph.D., Department of Sensory and Motor System Medicine, University of Tokyo, Hongo 7-3-1, Bunkyo-ku, Tokyo 113-8655, Japan. E-mail: kawaguchi-ort@h.u-tokyo.ac.jp.

This work was supported by Grants-in-Aid for Scientific Research nos. 11470301 and 12137201 from the Japanese Ministry of Education, Science, Sports, Culture and Technology.

References

1. Dempster DW, Cosman F, Parisien M, Shen V, Lindsay R 1994 Anabolic actions of parathyroid hormone on bone. Endocr Rev 15:261–280
2. Eastell R 1998 Treatment of postmenopausal osteoporosis. N Engl J Med 338:736–745
3. Neer RM, Arnaud CD, Zanchetta JR, Prince R, Gaich GA, Reginster JY, Hodsman AB, Eriksen EF, Ish-Shalom S, Genant HK, Wang O, Mitlak BH 2001 Effect of parathyroid hormone (1–34) on fractures and bone mineral density in postmenopausal women with osteoporosis. N Engl J Med 344:1434–1441
4. Rosen CJ 2003 The cellular and clinical parameters of anabolic therapy for osteoporosis. Crit Rev Eukaryot Gene Expr 13:25–38
5. Isogai Y, Akatsu T, Ishizuya T, Yamaguchi A, Hori M, Takahashi N, Suda T 1996 Parathyroid hormone regulates osteoblast differentiation positively or negatively depending on the differentiation stages. J Bone Miner Res 11:1384–1393
6. Nishida S, Yamaguchi A, Tanizawa T, Endo N, Mashiba T, Uchiyama Y, Suda T, Yoshiki S, Takahashi E 1994 Increased bone formation by intermittent parathyroid hormone administration is due to the stimulation of proliferation and differentiation of osteoprogenitor cells in bone marrow. Bone 15:717–723
7. Jilka RL, Weinstein RS, Bellido T, Roberson P, Parfitt AM, Manolagas SC 1999 Increased bone formation by prevention of osteoblast apoptosis with parathyroid hormone. J Clin Invest 104:439–446
8. McCarthy TL, Centrella M, Canalis E 1989 Parathyroid hormone enhances the transcript and polypeptide levels of insulin-like growth factor I in osteoblast-enriched cultures from fetal rat bone. Endocrinology 124:1247–1253
9. Watson P, Lazowski D, Han V, Fraher L, Steer B, Hodsman A 1995 Parathyroid hormone restores bone mass and enhances osteoblast insulin-like growth factor I gene expression in ovariectomized rats. Bone 16:357–365
10. Canalis E 1993 Insulin like growth factors and the local regulation of bone formation. Bone 14:273–276
11. Canalis E, Centrella M, Burch W, McCarthy TL 1989 Insulin-like growth factor I mediates selective anabolic effects of parathyroid hormone in bone cultures. J Clin Invest 83:60–65
12. Ishizuya T, Yokose S, Hori M, Noda T, Suda T, Yoshiki S, Yamaguchi A 1997 Parathyroid hormone exerts disparate effects on osteoblast differentiation depending on exposure time in rat osteoblastic cells. J Clin Invest 99:2961–2970
13. Miyakoshi N, Kasukawa Y, Linkhart TA, Baylink DJ, Mohan S 2001 Evidence that anabolic effects of PTH on bone require IGF-I in growing mice. Endocrinology 142:4349–4356
14. Bikle DD, Sakata T, Leary C, Elalieh H, Ginzinger D, Rosen CJ, Beamer W, Majumdar S, Halloran BP 2002 Insulin-like growth factor I is required for the anabolic actions of parathyroid hormone on mouse bone. J Bone Miner Res 17:1570–1578
15. Kadowaki T, Tobe K, Honda-Yamamoto R, Tamemoto H, Kaburagi Y, Momomura K, Ueki K, Takahashi Y, Yamauchi T, Akanuma Y, Yazaki Y 1996 Signal transduction mechanism of insulin and insulin-like growth factor-1. Endocr J 43:S33–S41
16. Ogata N, Chikazu D, Kubota N, Terauchi Y, Tobe T, Azuma Y, Ohta T, Kadowaki T, Nakamura K, Kawaguchi H 2000 Insulin receptor substrate-1 in osteoblast is indispensable for maintaining bone turnover. J Clin Invest 105:935–943
17. Akune T, Hoshi K, Kubota Y, Terauchi K, Tobe Y, Azuma T, Ohta T, Nakamura K, Kawaguchi H 2002 Insulin receptor substrate-2 maintains predominance of anabolic function over catabolic function of osteoblasts. J Cell Biol 159:147–156
18. Parfitt AM, Drezner MK, Glorieux FH, Kanis JA, Malluche H, Meunier PJ, Ott SM, Recker RR 1987 Bone histomorphometry: standardization of nomenclature, symbols, and units. Report of the ASBMR Histomorphometry Nomenclature Committee. J Bone Miner Res 2:595–610
19. Tamemoto H, Kadowaki T, Tobe K, Yagi T, Sakura H, Hayakawa T, Terauchi Y, Ueki K, Kaburagi Y, Satoh S, Nagai R, Yazaki T 1994 Insulin resistance and growth retardation in mice lacking insulin receptor substrate-1. Nature 372:182–186
20. Kubota N, Tobe K, Terauchi Y, Eto K, Yamauchi T, Suzuki R, Tsubamoto Y, Komeda K, Nakano R, Miki H, Satoh S, Sekihara H, Sciacchitano S, Lesniak M, Aizawa S, Nagai R, Kimura S, Akanuma Y, Taylor SI, Kadowaki T 2000 Disruption of insulin receptor substrate 2 causes type 2 diabetes because of liver insulin resistance and lack of compensatory β-cell hyperplasia. Diabetes 49:1880–1889
21. Hoshi K, Ogata N, Shimoaka T, Terauchi Y, Kadowaki T, Kenmotsu S, Chung UI, Ozawa H, Nakamura K, Kawaguchi H 2004 Deficiency of insulin receptor substrate-1 impairs skeletal growth through early closure of epiphyseal cartilage. J Bone Miner Res 19:214–223
22. Bruning JC, Winnay J, Cheatham B, Kahn CR 1997 Differential signaling by insulin receptor substrate 1 (IRS-1) and IRS-2 in IRS-1-deficient cells. Mol Cell Biol 17:1513–1521
23. Shimoaka T, Kamekura S, Chikuda H, Hoshi K, Chung UI, Akune T, Maruyama Z, Komori T, Matsumoto M, Ogawa W, Terauchi Y, Kadowaki T, Nakamura K, Kawaguchi H 2004 Impairment of bone healing by insulin receptor substrate-1 deficiency. J Biol Chem 279:15314–15322
24. Sato M, Westmore M, Ma YL, Schmidt A, Zeng QQ, Glass EV, Vahle J, Brommage R, Jerome CP, Turner CH 2004 Teriparatide [PTH(1–34)] strengthens the proximal femur of ovariectomized nonhuman primates despite increasing porosity. J Bone Miner Res 19:623–629
25. Dempster DW, Cosman F, Kurland ES, Zhou H, Nieves J, Woelfert L, Shane E, Plavetic K, Muller R, Bilezikian J, Lindsay R 2001 Effects of daily treatment with parathyroid hormone on bone microarchitecture and turnover in patients with osteoporosis: a paired biopsy study. J Bone Miner Res 16:1846–1853
26. Black DM, Greenspan SL, Ensrud KE, Palermo L, McGowan JA, Lang TF, Garnero P, Bouxsein ML, Bilezikian JP, Rosen CJ; PTH Study Investigators

2003 The effects of parathyroid hormone and alendronate alone or in combination in postmenopausal osteoporosis. N Engl J Med 349:1207–1215
27. **Finkelstein JS, Hayes A, Hunzelman JL, Wyland JJ, Lee H, Neer RM** 2003 The effects of parathyroid hormone, alendronate, or both in men with osteoporosis. N Engl J Med 349:1216–1226
28. **Umayahara Y, Billiard J, Ji C, Centrella M, McCarthy TL, Rotwein P** 1999 CCAAT/enhancer-binding protein δ is a critical regulator of insulin-like growth factor-I gene transcription in osteoblasts. J Biol Chem 274:10609–10617
29. **Chang W, Rewari A, Centrella M, McCarthy TL** 2004 Fos-related antigen 2 controls protein kinase A-induced CCAAT/enhancer-binding protein β expression in osteoblasts. J Biol Chem 279:42438–42444
30. **Swarthout JT, Doggett TA, Lemker JL, Partridge NC** 2001 Stimulation of extracellular signal-regulated kinases and proliferation in rat osteoblastic cells by parathyroid hormone is protein kinase C-dependent. J Biol Chem 276: 7586–7592
31. **Gentili C, Morelli S, Russo De Boland A** 2002 Involvement of PI3-kinase and its association with c-Src in PTH-stimulated rat enterocytes. J Cell Biochem 86:773–783
32. **Lee K, Deeds JD, Chiba S, Un-No M, Bond AT, Segre GV** 1994 Parathyroid hormone induces sequential c-*fos* expression in bone cells in vivo: *in situ* localization of its receptor and c-*fos* messenger ribonucleic acids. Endocrinology 134:441–450
33. **Merriman HL, La Tour D, Linkhart TA, Mohan S, Baylink DJ, Strong DD** 1990 Insulin-like growth factor-I and insulin-like growth factor-II induce c-*fos* in mouse osteoblastic cells. Calcif Tissue Int 46:258–262
34. **Onishi T, Zhang W, Cao X, Hruska K** 1997 The mitogenic effect of parathyroid hormone is associated with E2F-dependent activation of cyclin-dependent kinase 1 (cdc2) in osteoblast precursors. J Bone Miner Res 12:1596–1605
35. **Furlanetto RW, Harwell SE, Frick KK** 1994 Insulin-like growth factor-I induces cyclin-D1 expression in MG63 human osteosarcoma cells *in vitro*. Mol Endocrinol 8:510–517
36. **Yakar S, Liu JL, Stannard B** 1999 Normal growth and development in the absence of hepatic insulin-like growth factor I. Proc Natl Acad Sci USA 96: 7324–7329
37. **Sjogren K, Liu JL, Blad K** 1999 Liver-derived insulin-like growth factor I (IGF-I) is the principal source of IGF-I in blood but is not required for postnatal body growth in mice. Proc Natl Acad Sci USA 96:7088–7092
38. **Ohlsson C, Bengtsson BA, Isaksson OG, Andreassen TT, Slootweg MC** 1998 Growth hormone and bone. Endocr Rev 19:55–79
39. **Gray TK, Mohan S, Linkhart TA, Baylink DJ** 1989 Estradiol stimulates *in vitro* the secretion of insulin-like growth factors by the clonal osteoblastic cell line, UMR106. Biochem Biophys Res Commun 158:407–412
40. **Cheng M, Zaman G, Rawlinson SC, Mohan S, Baylink DJ, Lanyon LE** 1999 Mechanical strain stimulates ROS cell proliferation through IGF-II and estrogen through IGF-I. J Bone Miner Res 14:1742–1750
41. **Gori F, Hofbauer LC, Conover CA, Khosla S** 1999 Effects of androgens on the insulin-like growth factor system in an androgen-responsive human osteoblastic cell line. Endocrinology 140:5579–5586
42. **Huang BK, Golden LA, Tarjan G, Madison LD, Stern PH** 2000 Insulin-like growth factor I production is essential for anabolic effects of thyroid hormone in osteoblasts. J Bone Miner Res 15:188–197

Endocrinology **is published monthly by The Endocrine Society (http://www.endo-society.org), the foremost professional society serving the endocrine community.**

Inhibition of Cdk6 Expression Through p38 MAP Kinase Is Involved in Differentiation of Mouse Prechondrocyte ATDC5

TORU MORO,[1] TORU OGASAWARA,[1] HIROTAKA CHIKUDA,[1] TOSHIYUKI IKEDA,[1] NAOSHI OGATA,[1] ZENJIRO MARUYAMA,[2] TOSHIHISA KOMORI,[2] KAZUTO HOSHI,[1] UNG-IL CHUNG,[1] KOZO NAKAMURA,[2] HIROTO OKAYAMA,[3] AND HIROSHI KAWAGUCHI[1]*

[1]*Department of Sensory and Motor System Medicine, Faculty of Medicine, University of Tokyo, Tokyo, Japan*

[2]*Division of Oral Cytology and Cell Biology, Nagasaki University Graduate School of Biomedical Sciences, Nagasaki, Japan*

[3]*Department of Biochemistry and Molecular Biology, Faculty of Medicine, University of Tokyo, Tokyo, Japan*

Because a temporal arrest in the G1-phase of the cell cycle is a prerequisite for cell differentiation, this study investigated the involvement of cell cycle factors in the differentiation of cultured mouse prechondrocyte cell line ATDC5. Among the G1 cell cycle factors examined, both protein and mRNA levels of cyclin-dependent kinase (Cdk6) were downregulated during the culture in a differentiation medium. The protein degradation of Cdk6 was not involved in this downregulation because proteasome inhibitors did not reverse the protein level. When inhibitors of p38 MAPK, ERK-1/2, and PI3K/Akt were added to the culture, only a p38 MAPK inhibitor SB203580 blocked the decrease in the Cdk6 protein level by the differentiation medium, indicating that the Cdk6 inhibition was mediated by p38 MAPK pathway. In fact, p38 MAPK was confirmed to be phosphorylated during differentiation of ATDC5 cells. Enforced expression of Cdk6 in ATDC5 cells blocked the chondrocyte differentiation and inhibited Sox5 and Sox6 expressions. However, the Cdk6 overexpression did not affect the proliferation or the cell cycle progression, suggesting that the inhibitory effect of Cdk6 on the differentiation was exerted by a mechanism largely independent of its cell cycle regulation. These results indicate that Cdk6 may be a regulator of chondrocyte differentiation and that its p38-mediated downregulation is involved in the efficient differentiation. J. Cell. Physiol. 204: 927–933, 2005. © 2005 Wiley-Liss, Inc.

Endochondral ossification is an essential process for embryonic development, skeletal growth, and fracture healing. This highly regulated process involves the coordination of chondrocyte proliferation and differentiation to give rise to the cartilaginous structures, which are subsequently replaced by bone (Karsenty and Wagner, 2002). Chondrocytes that are derived from mesenchymal cells proliferate to expand the cartilage mold, and then form columns of flattened proliferative cells. Chondrocytes then permanently exit the cell cycle, and postmitotic cells further differentiate into prehypertrophic and hypertrophic chondrocytes, which secrete an extracellular matrix that becomes mineralized. Analyses of transgenic and knockout mice have demonstrated that disturbance of the fine balance between chondrocyte proliferation and differentiation can cause skeletal defects such as skeletal dysplasias (Mundlos and Olsen, 1997a,b; Serra et al., 1997). Thus, in this process of endochondral bone formation, proliferation and differentiation of chondrocytes must be properly coordinated; however, the molecular processes regulating these functions remain largely unknown.

Cell cycle factors appear to play an important role in the control of chondrocyte proliferation and differentiation (Beier et al., 1999a; LuValle and Beier, 2000). Proliferation of eukaryotic cells depends on their progression through the cell cycle, and at least a temporal cell cycle arrest at the G1-phase is thought to be a prerequisite for cell differentiation (Sherr, 1994). Complexes of cyclin and cyclin-dependent kinase (Cdk) promote G1/S-phase transition by phosphorylating the retinoblastoma (Rb) pocket protein family members Rb, p107, and p130. Phosphorylation of the pocket protein blocks their ability to repress E2F family members, leading to activation of genes required for S-phase entry. The predominant G1 cyclin–Cdk complexes are cyclin D-Cdk4/6, and in late G1, cyclin E-Cdk2. The D-type cyclins are upregulated by mitogenic stimuli (Coqueret, 2002), and cyclin–Cdk complexes are inhibited by two major families of Cdk inhibitors (CKIs) (Sherr and Roberts, 1999). The INK4 family specifically binds and inactivates monomeric Cdk4 or Cdk6, whereas the CiP/KiP family, which includes p21, p27, and p57, inhibits all G1/S-phase cyclin–Cdk complexes, except for the cyclin D3–Cdk6 complex (Lin et al., 2001).

Since in lower eukaryotes the control of cell cycle factors driving S-phase onset greatly influences the commitment to cell differentiation, the present study investigated the possibility of crucial participation of these factors in chondrocyte differentiation using a mouse prechondrocyte cell line ATDC5, and found that in the differentiation medium containing insulin Cdk6 was downregulated primarily by p38 mitogen-activated protein kinase (MAPK) signal-invoked transcriptional

Contract grant sponsor: Japanese Ministry of Education, Culture, Sports, Science, and Technology; Contract grant numbers: 14657358, 16659402.

*Correspondence to: Hiroshi Kawaguchi, Department of Sensory and Motor System Medicine, Faculty of Medicine, University of Tokyo, Hongo 7-3-1, Bunkyo, Tokyo 113-8655, Japan.
E-mail: kawaguchi-ort@h.u-tokyo.ac.jp

Received 10 September 2004; Accepted 7 January 2005

Published online in Wiley InterScience (www.interscience.wiley.com.), 28 March 2005.
DOI: 10.1002/jcp.20350

repression and that its down-regulation was involved in the efficient differentiation.

MATERIALS AND METHODS

Reagents and antibodies

Insulin-transferrin-sodium selenite supplement (ITS) was purchased from Roche Molecular Biochemicals (Mannheim, Germany). Antibodies against Cdk2 (H-298), Cdk4 (C-22), Cdk6 (C-21), cyclin A (C-19), cyclin D1 (C-20), cyclin D2 (M-20), cyclin D3 (C-16), cyclin E (M-20), p15 (K-18), p16 (H-156), p18 (M-20), p19 (M-20), p21 (M-19), p27 (F-8), and p57 (C-20) were obtained from Santa Cruz Biotechnology (Santa Cruz, CA). Antibodies against p38 MAPK (#9212) and phosphorylated p38 MAPK (#9211S) were purchased from Cell Signaling Technology, Inc. (Beverly, MA). Antibodies against β-actin (AC-15) were purchased from Sigma Chemical Co. (St. Louis, MO). 4-(4-fluorophenyl)-2-(4-methylsulfinylphenyl)-5-(4-pyridyl)-1H-imidazole (SB203580), 2-(4-morpholinyl)-8-phenyl-4H-1-benzopyran-4-one (LY294002), and 2′-Amino-3′-methoxyflanone (PD98059) were purchased from Calbiochem Novabiochem Co. (La Jolla, CA).

Cell culture

Mouse prechondrocyte cell line ATDC5 cells were purchased from the Riken Cell Bank (Tsukuba, Japan). The cells were maintained in Dulbecco's minimal essential medium nutrient mixture F-12 HAM (DMEM/F12; Sigma) containing 5% fetal bovine serum (FBS; Sigma) in 5% CO_2 in air. For induction of chondrogenesis, cells were inoculated at 5×10^4 cells in a 6-well plate or 5×10^5 cells in a 10-cm diameter plate with the culture medium changed to DMEM without FBS, and were precultured under serum starvation for 24–48 h. The growth-arrested ATDC5 cells were then stimulated with 5% FBS in the presence or absence of ITS (10 μg/ml insulin, 10 μg/ml transferrin, and 3×10^{-8} M sodium selenite) for 6–72 h. To block protein degradation, we added the proteasome inhibitors MG132 (2 μM, *Z*-Leu-Leu-Leu-aldehyde; Peptide Institute, Osaka, Japan) and lactacystin (20 μM, Calbiochem Novabiochem Co.) to the experimental medium, as previously reported (Urano et al., 1999; Ogasawara et al., 2004b). To block p38 MAPK, extracellular signal-regulated kinase (ERK)-1/2, and phosphatidylinositol 3 kinase (PI3K)/Akt pathways, we used SB203580 (30 μM), PD98059 (20 μM), and LY294002 (40 μM), respectively (Nakamura et al., 1999; Hidaka et al., 2001; Watanabe et al., 2001).

Construction of cell clones constitutively expressing Cdk6

ATDC5 cells were inoculated at 5×10^5 cells per 6-cm diameter plate, incubated for 24 h, and then transfected with the pEF/neo I vector carrying a human *Cdk6* cDNA or no insert by use of the Lipofectamine reagent (Life Technologies, Inc., Grand Island, NY) according to the manufacturer's instructions. Twenty-four hours later, the cells were split 1:10 to 1:100 and selected in DMEM/F12 containing 5% FBS and 200 μg/ml of G418 (Geneticin; Life Technologies, Inc.). Stable G418-resistant colonies were then isolated and expanded for 2 weeks in the medium above. The levels of Cdk6 were then quantified by Western blotting to select high expressing and low expressing clones. Cells with less than 1.5-fold of Cdk6 protein levels compared to the empty vector (EV)-transfected cells, determined by densitometry (Bio-Rad Laboratories, Richmond, CA), were defined as low expressers and those with more than fivefold of EV cells as high expressers. To know the effect of ITS on the Cdk6 overexpression level, Western blotting was performed after 5 weeks of additional culture in the presence of ITS. Cdk2 and Cdk4 levels were also examined in both situations.

Western blot analysis

The cells were rinsed with ice-cold phosphate-buffered saline (PBS) and lysed with RIPA buffer (10 mM Tris-HCl [pH 7.5], 150 mM NaCl, 1% Nonidet P-40 [NP-40], 0.1% sodium dodecyl sulfate [SDS], 10 μg of aprotinin/ml, 0.1 M NaF, 2 mM Na3VO4, and 1% Na deoxycholate). After a brief sonication, the lysed cells were centrifuged at 15,000*g* for 20 min at 4°C to obtain soluble cell extracts. The protein concentration in the cell lysate was measured using a Protein Assay Kit II (Bio-Rad). The cell extracts (10 μg of protein each) were separated by SDS-7.5, 10, or 12.5% polyacrylamide gel electrophoresis and electrotransferred to polyvinylidene difluoride membranes (Immobilon-P; Millipore Corp., Bedford, MA). After the blocking of nonspecific binding by soaking of the filters in 5% skim milk, the desired proteins were immunodetected with their respective antibodies, followed by visualization using the ECL Plus Western blotting detection system (Amersham Pharmacia Biotech, Buckinghamshire, UK) according to the manufacturer's instructions.

Reverse transcription-PCR (RT-PCR)

Total RNA (1 μg) was extracted from cells using ISOGEN (Wako Pure Chemicals, Osaka, Japan) following the manufacturer's instructions, reverse transcribed using SUPERSCRIPT First-Strand Synthesis System for RT-PCR (Life Technologies, Inc.), and amplified within an exponential phase of the amplification with a Perkin Elmer PCR Thermal Cycler (PE-2400). The gene-specific primer pairs used were as follows: 5′-CGTGGTCAGGTTGTTTGATG-3′ and 5′-TGCGAAACATTTCTGCAAAG-3′ for Cdk6, 5′-AGTAACTTCGTGCCTAGCAA-3′ and 5′-TCCTTTCACGCCTTTGAAGC-3′ for type II collagen (COL2), 5′-AGGCAAGCCAGGCTATGGAA-3′ and 5′-GCTGTCCTGGAAAGCCGTTT-3′ for type X collagen (COL10), 5′-CATGTAGGCCATGAGGTCCACCAC-3′ and 5′-TGAAGGTCGGTGTGAACGGATTTGGC-3′ for glyceraldehyde-3-phosphate dehydrogenase (GAPDH). The cycling parameters were 30 sec at 94°C, 30 sec at 55°C, and 90 sec at 72°C for Cdk6 and GAPDH; and 30 sec at 94°C, 30 sec at 60°C, and 90 sec at 72°C for COL2 and COL10.

Real-time quantitative RT-PCR

Total RNA extracted as described above was reverse-transcribed with Takara RNA PCR Kit (AMV) ver.2.1 (Takara, Tokyo, Japan) to generate single-stranded cDNA. PCR was performed with an ABI Prism 7000 Sequence Detection System (Applied Biosystems, Foster, CA). PCR reactions consisted of 1× QuantiTect SYBR Green PCR Master Mix (Qiagen, Hilden, Germany), 0.3 μM specific primers, and 500 ng of cDNA. mRNA copy number of a specific gene in each total RNA was calculated with a standard curve generated with serially diluted plasmids containing PCR amplicon sequences, and normalized to the rodent total RNA (Applied Biosystems) with β-actin as an internal control. Standard plasmids were synthesized with TOPO TA Cloning Kit (Invitrogen, Carlsbad, CA) according to the manufacturer's instruction. All reactions were run in triplicate. Primer sequences for Sox5 were, sense (5′-CTCGCTGGAAAGCTATGACC-3′) and antisense (5′-GATGGGGATCTGTGCTTGTT-3′), for Sox6 were, sense (5′-GGATTGGG- GAGTACAAGCAA-3′) and antisense (5′-CATCTGAGGTGATGGTGTGG-3′), for Sox9 were, sense (5′-CGACTACGCTGACCATCAGA-3′) and antisense (5′-AGACTGGTTGTTCCCAGTGC-3′), and for β-actin were, sense(5′-AGATGTGGATCAGCAAGCAG-3′) and antisense (5′-GCGCAAGTTAGGTTTTGTCA-3′).

Alcian blue, alizarin red, and alkaline phosphatase (ALP) stainings

ATDC5 cells were inoculated at 5×10^4 cells per well in a 6-well plate and cultured in DMEM/F12 containing 5% FBS in 5% CO_2 in air. After being cultured to be subconfluent, the cells were induced for differentition by adding 10 μg/ml ITS and cultured for 3 weeks, then the culture medium was changed to α-minimum essential medium (αMEM; Life Technologies, Inc.) containing 5% FBS with ITS, and the cells were cultured in 3% CO_2 in air for more 2 weeks. Alcian blue staining was done at 3 weeks after induction of chondrogenesis, and Alizarin red and ALP stainings at 5 weeks. For Alcian blue staining, the cells were rinsed with PBS, fixed with 10% (vol/vol) formaldehyde, and stained with 0.3% Alcian blue 8GS (Fluka, Buchs, Switzerland) in 0.1 N HCl. For Alizarin red staining, the cells were rinsed with PBS and fixed with 10% (vol/vol) formaldehyde, and were stained

with 1% Alizarin red S (pH 4.0) (Sigma). For ALP staining, the cells were rinsed with PBS and fixed with 70% ethanol in PBS and then stained with naphthol AS-MX phosphate (Sigma) as a substrate in *N,N*-dimethyl formamide, and Fast BB salt (Sigma) as a coupler.

BrdU incorporation assay

ATDC5 cells were inoculated at 10^3 cells per well in a 96-well plate and cultured in DMEM/F12 containing 5% FBS with or without ITS. After 72 h of culture, the cells were labeled with bromodeoxyuridine (BrdU) for 2 h, and the cell population entering S-phase was determined by quantifying the incorporated BrdU (Cell Proliferation ELISA; Roche Molecular Biochemical) according to the manufacturer's instructions.

Flow cytometric analysis

After 72 h of culture, approximately 10^5 cells were suspended in 0.02 ml of citrate buffer and subjected to the following serial treatments at room temperature: (i) the addition of 0.18 ml of solution A (0.03 mg of trypsin/ml, 3.4 mM trisodium citrate, 0.1% NP-40, 1.5 mM spermine-4HCl, and 0.5 mM Tris-HCl [pH 7.6]) and incubation for 10 min; (ii) the addition of 0.15 ml of solution B (3.4 mM trisodium citrate, 0.1% NP-40, 1.5 mM spermine-4HCl, 0.5 mM Tris-HCl [pH 7.6], 0.5 mg of trypsin inhibitor/ml, 0.1 mg of RNase A/ml) and incubation for 10 min; and (iii) the addition of 0.15 ml of solution C (4.16 mg of propidium iodide/ml, 3.4 mM trisodium citrate, 0.1% NP-40, 4.8 mM spermine-4HCl, 0.5 mM Tris-HCl [pH 7.6]) and incubation for 10 min. The DNA content was determined and analyzed with EPICS XL and XL EXPO32 instruments (Beckman, Fullerton, CA).

Statistical analysis

The means of groups were compared by analysis of variance, and the significance of differences was determined by posthoc testing using the Bonferroni method.

RESULTS

Downregulation of Cdk6 during differentiation of ATDC5 cells

Considering that ATDC5 cells begin to express COL2, a representative marker of chondrocytes, within 72–96 h of culture in the medium containing ITS, a putative inducer of chondrocyte differentiation (Shukunami et al., 1996, 1998), we assumed that the commitment of this cell line to differentiation occurred well within 72 h, and therefore analyzed the effect of ITS on the initial 72 h expression levels of cell cycle factors that critically regulate the onset of S-phase. The cells were arrested in quiescence by serum starvation, stimulated with serum in the presence or absence of ITS, and the amounts of cyclins (A, D1, D2, D3, and E), Cdk2, Cdk4, Cdk6, and CKIs (p15, p16, p18, p19, p21, p27, and p57) in the whole cell lysate at each time point were analyzed every 12–24 h by Western blotting (Fig. 1A). Interestingly, only Cdk6 protein level was significantly decreased by ITS at 24 h of culture and thereafter, while other Cdks, cyclins, and CKIs were hardly affected by the stimulation. Although Cdk4 and Cdk6 have about 70% homology of amino acid sequence (Meyerson et al., 1992) and share D cyclins as their catalytic partners, only Cdk6 was regulated, indicating that Cdk6 was specifically downregulated during the chondrocyte differentiation. To know the regulation of Cdk6 at the transcriptional level, we performed a semiquantitative RT-PCR analysis of the Cdk6 transcript and found that the mRNA level was also decreased when ATDC5 cells were stimulated with ITS (Fig. 1B). To further examine the involvement of the ubiquitin-proteasome pathway in the decreased Cdk6 protein level, ATDC5 cells were cultured with MG132 and lactacystin, potent proteasome inhibitors (Fig. 1C). These inhibitors did not affect the Cdk6 downregulation by ITS, suggesting that the effect of ITS was not due

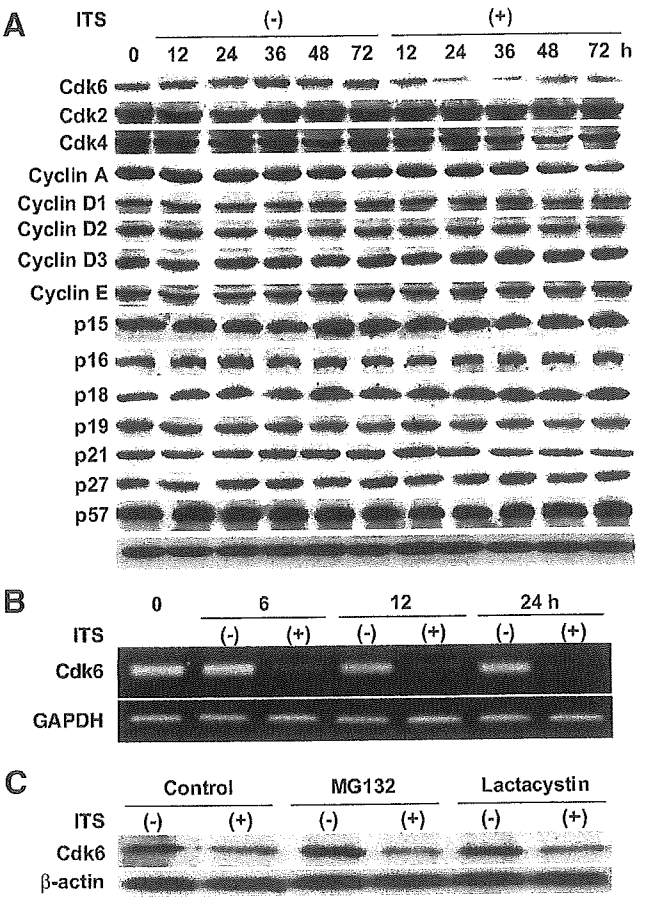

Fig. 1. Downregulation of Cdk6 during differentiation of ATDC5 cells. Growth-arrested ATDC5 cells were stimulated with 5% FBS in the presence or absence of ITS, a putative inducer of chondrocyte differentiation, and cell sampling was done at the indicated times. **A**: Time course of protein levels of cell cycle factors Cdks, cyclins, and CKIs, controlling the G1-S transition in ATDC5 cells during differentiation induction by ITS. The amounts of cell cycle factors were determined by Western blotting. β-actin was used as a loading control. **B**: Time course of the mRNA level of Cdk6 by a semiquantitative RT-PCR analysis in ATDC5 cells during differentiation by ITS. GAPDH was used as a loading control. **C**: Effects of proteasome inhibitors MG132 (2 μM) and lactacystin (20 μM) on the decreased Cdk6 protein level determined by Western blotting during ATDC5 cell differentiation by ITS. Growth-arrested ATDC5 cells were stimulated for 24 h, and the amounts were determined by Western blotting. β-actin was used as a loading control. In each figure a representative blotting is shown among at least three independent experiments that showed similar results.

to protein degradation by the ubiquitin-proteasome pathway. These findings indicate that the decreased Cdk6 expression during chondrocyte differentiation was mainly, if not exclusively, by transcriptional suppression.

Mediation of p38 MAPK in the downregulation of Cdk6

Since insulin, the principal factor in ITS for chondrocyte differentaition, is known to initiate cellular responses by binding to distinct cell-surface receptor tyrosine kinases that regulate a variety of signaling pathways such as those of MAPK and PI3K/Akt (Kadowaki et al., 1996), we examined the involvement of these pathways in the mechanism of the Cdk6 downregulation by ITS. Western blotting showed that ITS induced the phosphyrylation of p38 MAPK in cultured ATDC5 cells, which was confirmed to be

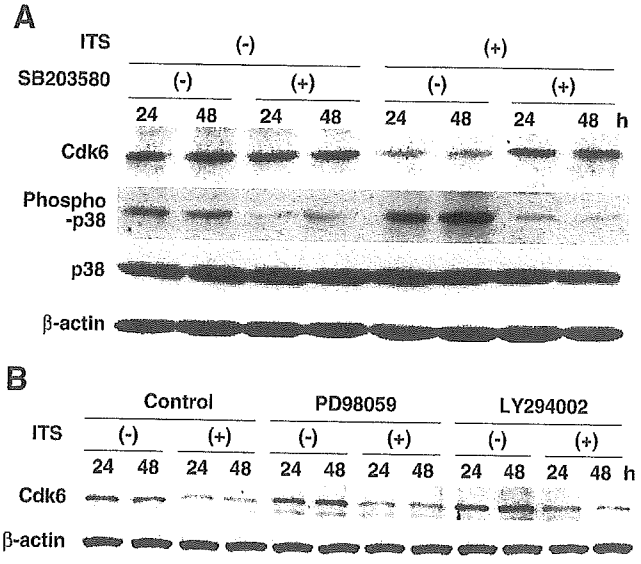

Fig. 2. Mediation of p38 MAPK, ERK-1/2, and PI3K/Akt pathways in the downregulation of Cdk6 during differentiation of ATDC5 cells. **A**: Effects of ITS and a p38 MAPK inhibitor SB203580 on the Cdk6 protein level and the p38 MAPK phosphorylation in the ATDC5 cell cultures. Growth-arrested ATDC5 cells were stimulated for 24 and 48 h, and the amounts were determined by Western blotting using specific antibodies. **B**: Effects of PD98059 and LY294002, inhibitors of ERK-1/2 and PI3K/Akt signalings, respectively, on the decreased Cdk6 protein level during ATDC5 cell differentiation by ITS. Growth-arrested ATDC5 cells were stimulated for 24 and 48 h, and the amounts were determined by Western blotting. In each figure a representative blotting is shown among at least four independent experiments that showed similar results. β-actin was used as a loading control.

blocked by SB203580, a p38 MAPK inhibitor (Fig. 2A). More importantly, SB203580 caused the restoration of the decreased Cdk6 protein level by ITS (Fig. 2A). On the other hand, PD98059 and LY294002, inhibitors of ERK-1/2 and PI3K/Akt signalings, respectively, did not alter the ITS-induced inhibition of the Cdk6 protein level (Fig. 2B). These findings demonstrate that downregulation of Cdk6 expression by ITS is at least partly mediated by the p38 MAPK pathway.

Impaired differentiation of ATDC5 cells overexpressing Cdk6

To further examine whether or not Cdk6 is functionally involved in chondrocyte differentiation, we generated ATDC5 cell clones stably overexpressing Cdk6 by transfecting with an expressing vector harboring *Cdk6* cDNA, and tested their ability to respond to ITS and differentiate to chondrocytes. We initially selected clones with low expression (#55 and #74) and high expression (#14 and #51), and confirmed that these overexpressions were maintained even after 5 weeks of culture in the presence of ITS (Fig. 3A). These overexpressions of Cdk6 affected neither the Cdk2 nor Cdk4 expression profiles even after long periods of culture with ITS (Fig. 3A). The ability of ITS to induce differentiation determined by Alcian blue, Alizarin red, and ALP stainings was then compared among the EV-transfected cells, low expressing cells, and high expressing cells after 3–5 weeks of culture. ITS induced the differentiation similarly in EV cells and low expressers; however, it was markedly decreased in high expressers (Fig. 3B). The ability of ITS to induce chondrocyte differentiation, as monitored by COL2 (Fig. 3C) and COL10 (Fig. 3D) mRNA levels by semiquantitative RT-PCR was further studied in the three kinds of transfected cells above. Here again, ITS strongly induced both COL2 and COL10 in the EV cells and low expressers, which was markedly decreased in high expressers. We further compared the expressions of Sox 5, Sox6, and Sox9, the key transcription factors for chondrogenic differentiation from precursors (Bi et al., 1999; Smits et al., 2001) by real-time quantitative RT-PCR analysis among the three kinds of transfected cells that were cultured for 24 h in the presence of ITS. The mRNA levels of Sox5 and Sox6, but not Sox9, were significantly lower in the high expressers than other two kinds of cells, indicating that Cdk6 exerts inhibitory action from an early stage of chondrocyte differentiation (Fig. 3E).

Unchanged cell cycle regulation of ATDC5 cells overexpressing Cdk6

Because Cdk6 promotes the G1-S transition, suppression of chondrocyte differentiation by overexpressed Cdk6 could be secondary to its execution of this role. We therefore examined the effect of Cdk6 overexpression on the proliferation and the G1-S transition of ATDC5 cells. The three kinds of transfected cells were similarly arrested in quiescence, stimulated with serum in the presence and absence of ITS, and analyzed for cell proliferation and populations in G0/G1 and G2/M by BrdU incorporation and FACS, respectively (Table 1). At 72 h of culture, when chondrocyte differentiation had just begun, ITS slightly increased the cell proliferation and the G2/M population; however, Cdk6 overexpression caused no significant changes in either of them. These results indicate that the inhibitory effect of Cdk6 on chondrocyte differentiation was not exerted via the cell cycle regulation.

DISCUSSION

In the present study, we have shown that Cdk6 expression is suppressed during differentiation of mouse prechondrocyte ATDC5 mainly at the transcriptional level and that this suppression, mediated by p38 MAPK signaling, is involved in the efficient differentiation. The work has demonstrated that Cdk6 plays a role in determining the differentiation rate of chondrocytes as a downstream effector of p38 MAPK signaling.

Although Cdk6 and Cdk4 and their partner D cyclins are all known to be critical factors controlling the cell growth potential (Baldin et al., 1993; Hengstschlager et al., 1999), several specific roles have been reported for Cdk6. The Cdk6–cyclin D3 complex is unique among cyclin D and cognate kinase combinations and evades inhibition by CKIs (Lin et al., 2001). Therefore, it can greatly enhance the proliferative potential of fibroblasts under growth-suppressive conditions (Lin et al., 2001) and, consequently, sensitizes cells to physical and chemical transformation (Chen et al., 2003). Cdk6 combined with cyclin K, encoded by human herpes virus 8 which is the causative agent of Kaposi sarcoma, is also reported to be immune to inhibition by CKIs (Swanton et al., 1997). These functions were not seen in Cdk4 complexes. This study also discovered a novel function of Cdk6 as an inhibitor of the transition to the differentiation stage without affecting the cell cycle regulation. Although Cdk4 has about 70% homology of amino acid sequence with Cdk6 (Meyerson et al., 1992), the Cdk4 protein level was not changed during ATDC5 differentiation in this study. We hereby propose that Cdk4 and Cdk6 play different roles and that Cdk4 cannot substitute for Cdk6 in chondrocyte differentiation.

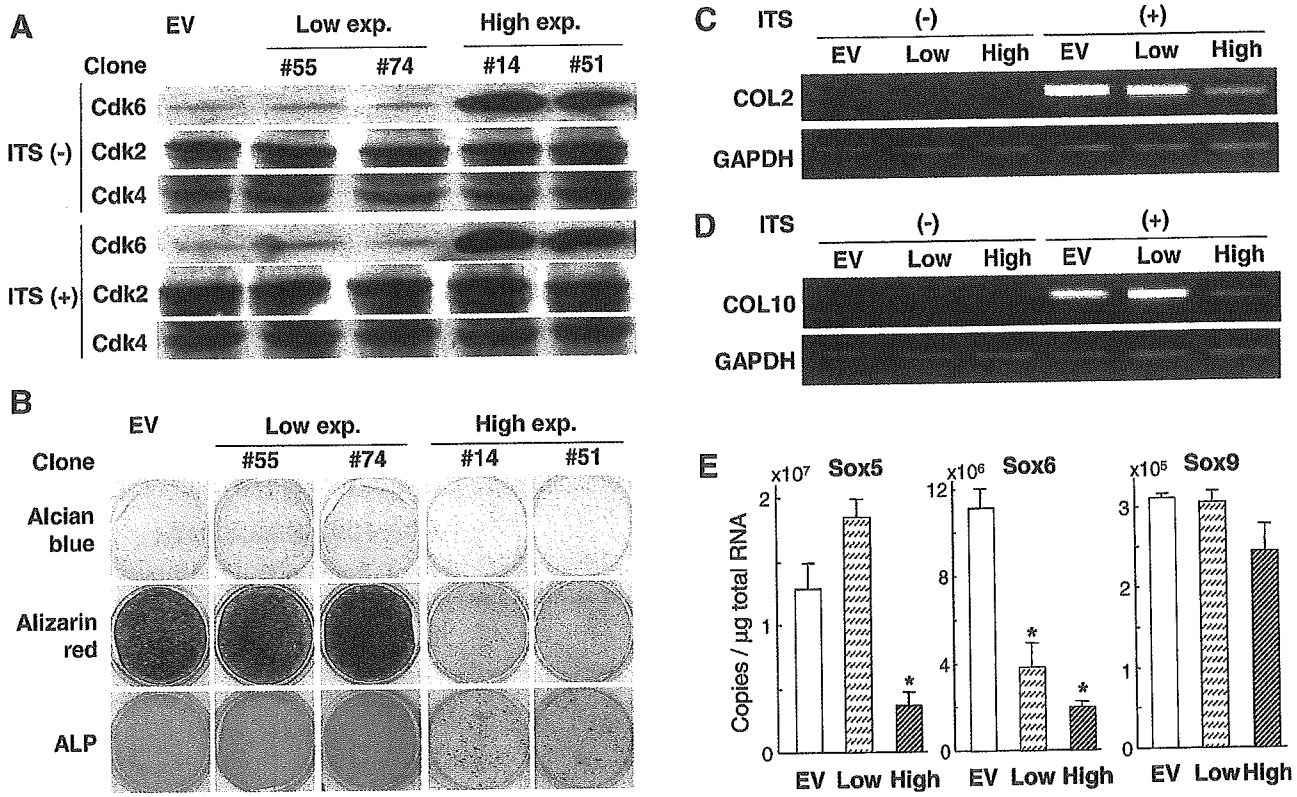

Fig. 3. Chondrocyte differentiation of ATDC5 cells with high and low expressions of Cdk6. **A**: Stable clones of ATDC5 cells transfected with *Cdk6* cDNA were isolated as described in Materials and Methods, and clones with low expression (#55 and #74) and high expression (#14 and #51) were selected on Western blotting after 2 weeks of expansion culture in the absence of ITS [ITS (−)]. To examine the effect of ITS on the Cdk6 overexpression, Western blotting was performed after 5 weeks of additional culture in the presence of ITS [ITS (+)]. **B**: Chondrocyte differentiation determined by Alcian blue, Alizarin red, and ALP stainings in the cultures of the low and high expressing clones, and empty vector (EV)-transfected ATDC5 cells under the induction of ITS for 3–5 weeks. **C**, **D**: mRNA levels of COL2 (C) and COL10 (D), as determined by semiquantitative RT-PCR, in EV cells, low expressers (#55), and high expressers (#14) cultured for 3 days and 14 days, respectively, in the presence or absence of ITS. GAPDH was used as a loading control. **E**: Expressions of Sox 5, Sox6, and Sox9, as determined by real-time quantitative RT-PCR analysis in EV cells, low expressers (#55), and high expressers (#14) cultured for 24 h in the presence of ITS. For (B–E), other clones with low and high expressions showed similar results.

The direct control of a factor(s) critically involved in the differentiation that is independent of cell cycle regulation, implicated as a Cdk6 action in this study, may not be as remote as generally thought. In fission yeast, Pas1 cyclin and its partner kinase Pef1 activate a transcriptional factor complex functionally equivalent to E2F-DP of mammals, thereby promoting S-phase entry just like Cdk6, yet they independently inhibit the mating pheromone signaling whose activation is essential for differentiation of this yeast cell (Tanaka and Okayama, 2000). Thus, this might be a good preceding model for the situation of Cdk6 in chondrocyte differentiation, highlighting a potential functional similarity between Cdk6 and Pef1.

Since Cdks are believed to have vital roles in controlling cell cycle progression among cell cycle factors, much attention has been devoted to the view that CKI-led inhibition of G1-specific Cdks is critical for cell differentiation. Recent reports have stated that some members of CKIs may function during the exit from the cell cycle and differentiation processes (Harper and Elledge, 1996; Chellappan et al., 1998). Overexpression of p21 and p27 has, in fact, promoted myogenesis, neurogenesis, and hematopoiesis (Liu

TABLE 1. Proliferation and cell cycle distribution of ATDC5 cells overexpressing Cdk6

	BrdU (OD)		FACS			
			G0/G1 (%)		G2/M (%)	
	ITS (−)	ITS (+)	ITS (−)	ITS (+)	ITS (−)	ITS (+)
EV	0.25 ± 0.01	0.35 ± 0.10	66.0 ± 0.6	62.7 ± 0.8	20.9 ± 0.2	23.6 ± 0.7
#55 (low)	0.23 ± 0.05	0.35 ± 0.09	65.6 ± 1.1	63.9 ± 0.7	22.4 ± 0.9	23.7 ± 0.5
#74 (low)	0.23 ± 0.03	0.39 ± 0.10	66.1 ± 0.1	64.8 ± 0.6	20.6 ± 0.5	22.5 ± 0.7
#14 (high)	0.20 ± 0.04	0.34 ± 0.11	66.3 ± 1.1	65.2 ± 0.5	20.4 ± 0.2	21.8 ± 0.7
#51 (high)	0.25 ± 0.01	0.36 ± 0.04	64.7 ± 1.2	62.6 ± 1.0	22.7 ± 0.3	24.7 ± 0.3

Cell proliferation was determined by BrdU incorporation into EV, low expressing and high expressing clones in the presence and absence of ITS at 72 h of culture. Cell cycle distribution was determined by FACS at 72 h of culture, and percentage of cells in each cell cycle stage (G0/G1 and G2/M) are shown. Data are expressed as the mean ± SD for 8 wells/clone. Cdk6 overexpression did not significantly affect the cell proliferation and the cell cycle distribution.